Biogenesis of cytochromes *c* and c_1 in the electron transport chain of malaria parasites

Aldo E. García-Guerrero†, Rebecca G. Marvin†, Amanda Mixon Blackwell†, and Paul A. Sigala*,†

†*Department of Biochemistry, University of Utah School of Medicine, Salt Lake City, UT, USA 84112*

*Corresponding author: Paul Sigala

E-mail: p.sigala@biochem.utah.edu

ABSTRACT

Plasmodium malaria parasites retain an essential mitochondrional electron transport chain (ETC) that is critical for growth within humans and mosquitoes and a key antimalarial drug target. ETC function requires cytochromes *c* and c_1 that are unusual among heme proteins due to their covalent binding to heme via conserved CXXCH sequence motifs. Heme attachment to these proteins in most eukaryotes requires the mitochondrial enzyme holocytochrome *c* synthase (HCCS) that binds heme and the apo cytochrome to facilitate biogenesis of the mature cytochrome *c* or c_1. Although humans encode a single bifunctional HCCS that attaches heme to both proteins, *Plasmodium* parasites are like yeast and encode two separate HCCS homologs thought to be specific for heme attachment to cyt *c* (HCCS) or cyt c_1 (HCC_1S). To test the function and specificity of *P. falciparum* HCCS and HCC_1S, we used CRISPR/Cas9 to tag both genes for conditional expression. HCC_1S knockdown selectively impaired cyt c_1 biogenesis and caused lethal ETC dysfunction that was not reversed by over-expression of HCCS. Knockdown of HCCS caused a more modest growth defect but strongly sensitized parasites to mitochondrial depolarization by proguanil, revealing key defects in ETC function. These results and prior heterologous studies in *E. coli* of cyt *c* hemylation by *P. falciparum* HCCS and HCC_1S strongly suggest that both homologs are essential for mitochondrial ETC function and have distinct specificities for biogenesis of cyt *c* and c_1, respectively, in parasites. This study lays a foundation to develop novel strategies to selectively block ETC function in malaria parasites.

INTRODUCTION

Malaria remains a devastating infectious disease, especially in sub-Saharan Africa [1]. The lack of a long-lasting, broadly protective vaccine and increasing resistance to frontline antimalarial drugs underscore the urgency to unravel the basic biology of malaria parasites to identify new vulnerabilities suitable for therapeutic targeting. Severe malaria is caused by *Plasmodium falciparum* parasites, which infect and grow asexually within human red blood cells (RBCs) to cause all malaria symptoms (**Fig. 1**). RBCs contain abundant hemoglobin with approximately 1 x 10^9 molecules of heme [2], and cellular metabolism involving this key cofactor is central to the biology of malaria parasites [3-5]. During their 48-hour residence inside an RBC, parasites internalize and digest nearly 80% of the host-cell hemoglobin [6]. This massive proteolysis releases copious free heme, which parasites detoxify by formation of hemozoin crystals inside their digestive vacuole. This critical pathway is a major antimalarial drug target and is central to the activity of chloroquine and artemisinin, two of the historically most successful antimalarial drugs [7].

P. falciparum parasites also require heme as a metabolic cofactor to support key aspects of their cellular physiology, especially the mitochondrial electron transport chain (ETC) that is essential for all stages of parasite development in humans and mosquitoes [4, 5, 8]. ETC activity is directly inhibited by the current antimalarial drug, atovaquone [9, 10], and the key vulnerability of this pathway in all parasite stages has made it the subject of intense drug discovery efforts [11-13]. Multiple heme-dependent cytochromes (cyt) are critical for ETC activity and parasite viability, including cyt *b* and c_1 in Complex III, soluble cyt *c* that shuttles electrons between Complexes III and IV, and the heme A-binding Cox1 subunit of Complex IV [4, 14]. In blood-stage parasites, the critical function of Complexes III and IV is oxidative recycling of the ubiquinone cofactor used as an electron acceptor by multiple mitochondrial dehydrogenases, especially dihydroorotate

dehydrogenase required for pyrimidine biosynthesis (**Fig. 1**) [10, 15-17]. Although electron transfer through these two complexes is accompanied by proton translocation across the inner membrane, this proton-pumping activity is not strictly essential for blood-stage parasites. *P. falciparum* has a redundant mechanism to polarize the mitochondrial inner membrane that is inhibited by proguanil, and blood-stage parasites rely on cytoplasmic glycolysis for ATP production rather than mitochondrial ATP synthase [10, 18]. Of the known mitochondrial cytochromes, cyt *b* and Cox1 are encoded on the mitochondrial genome, which is not currently accessible to genetic modification. Cyt *c* (Pf3D7_1404100) and c_1 (Pf3D7_1462700), however, are encoded in the nucleus, and we recently demonstrated that both cytochromes are critical for blood-stage parasites and ETC function [17]. *P. falciparum* and other apicomplexan parasites also encode a divergent cyt *c* paralog (cyt *c*-2, Pf3D7_1311700) that binds heme but whose function is dispensable for blood-stage parasites [17].

Mitochondrial cyt *c* and c_1, which are retained by nearly all aerobic eukaryotes, are distinguished from most heme proteins by their use of a conserved CXXCH sequence motif to covalently bind heme via formation of stable thioether bonds between the Cys residues and the heme vinyl groups [19-22]. In most eukaryotes, the assembly of these heme-bound cytochromes requires the enzyme holocytochrome *c* synthase (HCCS) that is located on the outer leaflet of the inner mitochondrial membrane and whose activity has been best studied in yeast and humans [23, 24]. Although hemylation of cyt *c* and c_1 is central to eukaryotic respiration, no structure has been determined experimentally for any mitochondrial HCCS from any organism. Nevertheless, recombinant expression and functional reconstitution of cyt *c* hemylation by human HCCS have enabled a proposed mechanism for heme attachment [24, 25]. According to this mechanism, HCCS binds heme via a conserved His residue, binds the N-terminal α-helix of apo cyt *c*, and positions

the bound heme proximal to the CXXCH residues to facilitate stereospecific heme attachment and thioether bond formation to cyt *c.* These steps are followed by folding and release of mature cyt *c*. Although humans and other metazoans retain a single bifunctional HCCS that can hemylate both cyt *c* and c_1 [26], other eukaryotes express two distinct HCCS homologs that preferentially hemylate cyt *c* (HCCS) or cyt c_1 (HCC_1S) [23, 27]. Nevertheless, studies in *Saccharomyces cerevisiae* [26] and the apicomplexan parasite *Toxoplasma gondii* [28] have suggested that HCCS in these organisms has limited promiscuous activity in hemylating cyt c_1, in addition to its preferred cyt *c* substrate.

P. falciparum also expresses both HCCS (Pf3D7_1224600) and HCC_1S (Pf3D7_1203600) homologs, but their functional properties have been sparsely studied. Genome-wide and targeted knock-out studies in *P. falciparum* and *P. berghei* have reported that both genes are refractory to disruption [29-31], suggesting non-redundant essential functions. Our prior work localized both proteins to the mitochondrion and also indicated that parasite HCCS but not HCC_1S could hemylate cyt *c* or *c*-2 when expressed heterologously in *E. coli*, suggesting that each homolog is specific for hemylating cyt *c* or c_1, respectively [17]. To directly test the function and specificity of HCCS and HCC_1S in *P. falciparum* parasites, we used CRISPR/Cas9 to tag each gene for conditional knockdown studies. Loss of HCC_1S impaired cyt c_1 biogenesis and resulted in lethal ETC dysfunctions that were not rescued by HCCS over-expression. Knockdown of HCCS led to a more modest phenotype but strongly sensitized parasites to mitochondrial depolarization by proguanil, unmasking a key ETC defect. These studies unravel non-overlapping critical functions for HCCS and HCC_1S in biogenesis of cyt *c* and c_1 in malaria parasites. Specificity differences between human and parasite HCCS homologs can provide a basis to develop selective inhibitors of ETC function in *Plasmodium*.

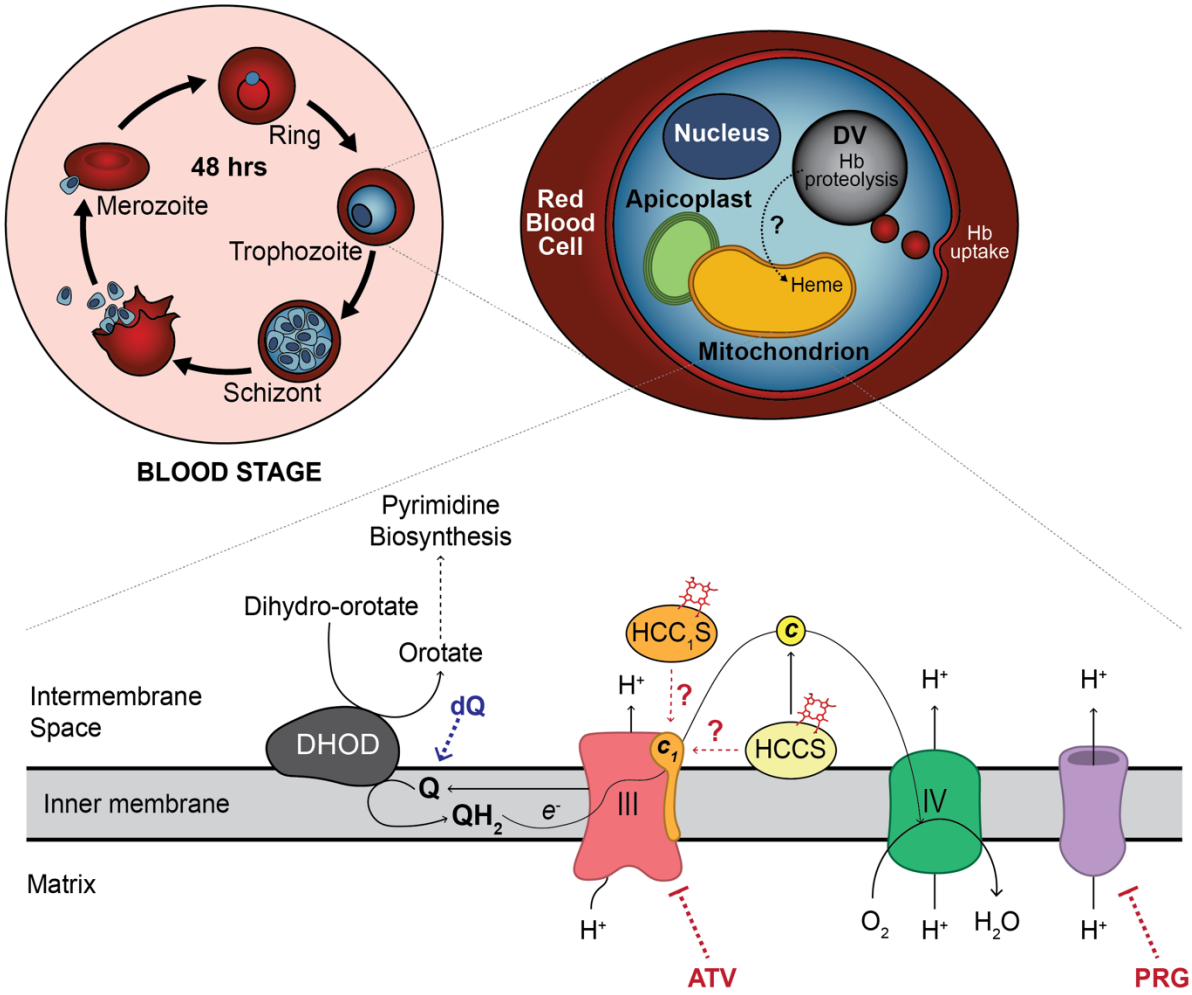

Figure 1. Schematic model of blood-stage infection and mitochondrial heme metabolism in *P. falciparum* parasites, focusing on the role of heme-dependent cytochromes *c* and c_1 in the electron transport chain. ATV = atovaquone, DHOD = dihydroorotate dehydrogenase, dQ = decyl-ubiquinone, DV = digestive vacuole, Hb = hemoglobin, Q = oxidized ubiquinone, QH_2 = reduced ubiquinol, III = Complex III/bc_1, IV = Complex IV/Cyt *c* oxidase, *c* = cyt *c*, c_1 = cyt c_1, HCCS = holocytochrome *c* synthase, HCC_1S, holocytochrome c_1 synthase, PRG = proguanil. Purple = alternative, proguanil-sensitive pathway for maintaining transmembrane potential. Question marks indicate functional uncertainty.

RESULTS

***P. falciparum* encodes HCCS and HCC_1S proteins homologous to yeast and humans.** To better understand the sequence features of the *Plasmodium* HCCS and HCC_1S homologs, we aligned these two proteins with HCCS orthologs from humans, yeast, and *Toxoplasma gondii* (**Fig. 2A**) and observed sequence identities ranging from 30-45%. *P. falciparum* HCCS (Pf3D7_1224600) had similar 35% and 38% sequence identity to yeast HCCS and HCC_1S, respectively. The parasite HCC_1S (Pf3D7_1203600), however, had higher sequence identity with yeast HCC_1S (41%) than yeast HCCS (30%), consistent with its predicted specificity for cyt c_1 and lack of detectable hemylation of cyt *c* in prior heterologous studies in *E. coli* [17]. We also generated a maximum likelihood phylogenetic tree, based on alignment of the *Plasmodium* HCCS and HCC_1S proteins with 52 orthologs from diverse eukaryotes, that further supported functional divergence between the parasite homologs (**Fig. 2B**).

Based on the alignment in Fig. 2A and in agreement with prior studies [24, 32], we observed multiple areas of strong sequence conservation between all orthologs that included the conserved His residues at H154 and H211 (Human HCCS numbering) and neighboring residues E159 and W162. H154 has previously been demonstrated in human HCCS to serve as a key axial ligand required for heme binding by HCCS and hemylation of cyt *c*, but a functional role for H211 remains undefined [24]. E159 and W162 also contribute to heme binding, and E159 mutations underpin the human disease called micropthalmia with linear skin defects syndrome [32, 33]. The high conservation in these and nearby residues between human and *P. falciparum* HCCS is consistent with our prior observation that each HCCS ortholog could promiscuously catalyze heme attachment to cyt *c* from both organisms [17].

No three-dimensional structure has been determined experimentally for a eukaryotic HCCS enzyme. As an initial step towards understanding structural features of HCCS, the positioning of conserved residues, and the possible orientation of HCCS bound to cyt *c* and its CXXCH heme-binding motif, we first turned to available AlphaFold models for human HCCS and *P. falciparum* HCCS and HCC_1S. Superposition of these structural models indicated very similar predicted structures for all three orthologs (**Fig. S1**), consistent with their substantial sequence similarity. The AlphaFold models suggest a central β-sheet that packs against an extended α-helix to create a central hydrophobic pocket, with several shorter α-helices predicted to pack around this hydrophobic core (**Fig. 3A and Fig. S1**). This predicted structure differs from a recent structural model for human HCCS generated by Rosetta and co-evolution approaches, which suggested a predominantly α-helical core structure [25]. Nevertheless, both models predict that H154 is positioned within the protein core, where this residue is expected to coordinate bound heme [24]. Indeed, AlphaFold 3 [34] modeled heme bound within the hydrophobic interior of parasite HCCS in an orientation coordinated by H154 (**Fig. S2**). The AlphaFold models further suggest that conserved H211 is positioned opposite H154 to possibly play a role as a second axial ligand for bound heme (**Fig. 3A and Fig. S2**). Prior mutagenesis studies with human HCCS found that H211 mutants showed minor reductions in heme attachment to cyt *c* that were less severe than H154 mutants [24], suggesting that H211 could contribute to heme binding to HCCS prior to association with apo cyt *c*. Such a role within the HCCS active site may underpin sequence conservation of H211 across phylogenetically disparate HCCS orthologs (**Fig. 2A**).

We noted that AlphaFold 3 generated two distinct models for heme-bound HCCS, differing in the position of a central α-helix that either exposed or occluded the bound heme (**Fig. S2**). In both conformations, a conserved Lys residue (K133) was positioned within 2-4 Å of a heme

propionate, suggesting a stabilizing electrostatic interaction that might underpin the strict conservation of this residue. The position of the central helix also appeared to pivot about a conserved Gly residue (G140), whose inherent conformational freedom may provide a flexible joint to enable rigid-body reorientation of this helix. The equilibrium distribution of these conformations gated by helical rearrangement may be critical for exposing the heme-bound HCCS active site for selective binding to the cyt *c* N-terminus during HCCS-catalyzed hemylation. Incisive tests of these hypotheses will require overcoming technical challenges to HCCS solubilization that have hampered experimental structure determination of this protein.

We next used AlphaFold 3 to model a possible complex between *P. falciparum* HCCS, heme, and the first 33 residues of the cyt *c* N-terminus, which include the N-terminal α-helix and CXXCH motif critical for recognition and heme attachment by HCCS [24, 35]. In the modeled protein complex (**Fig. 3B**), which AlphaFold 3 generated based only on the input amino acid sequences and selecting heme as ligand, the N-terminal α-helix of cyt *c* packs against and perpendicular to one end of the central α-helix of HCCS. This orientation positions the conserved Cys residues of the CXXCH motif proximal to the active site cavity such that the conserved cyt *c* His residue (H19 in human numbering) extends into the HCCS active site and replaces H211 of HCCS in an orientation opposite H154. AlphaFold 3 modeled heme bound within the hydrophobic core of HCCS with the central iron coordinated by H154 of HCCS and the conserved H19 of cyt *c* such that the vinyl groups of heme were positioned proximal to C16 and C18 of cyt *c* (**Fig. 3B**). This model suggests a key intermediate in cyt *c* hemylation in which HCCS-bound heme is positioned by opposing His coordination to facilitate thioether bond formation between the Cys residues of cyt *c* and heme vinyl groups. This model is consistent with prior mechanistic suggestions for

human HCCS maturation of cyt *c* based on biochemical experiments and structural modeling [24, 25, 36].

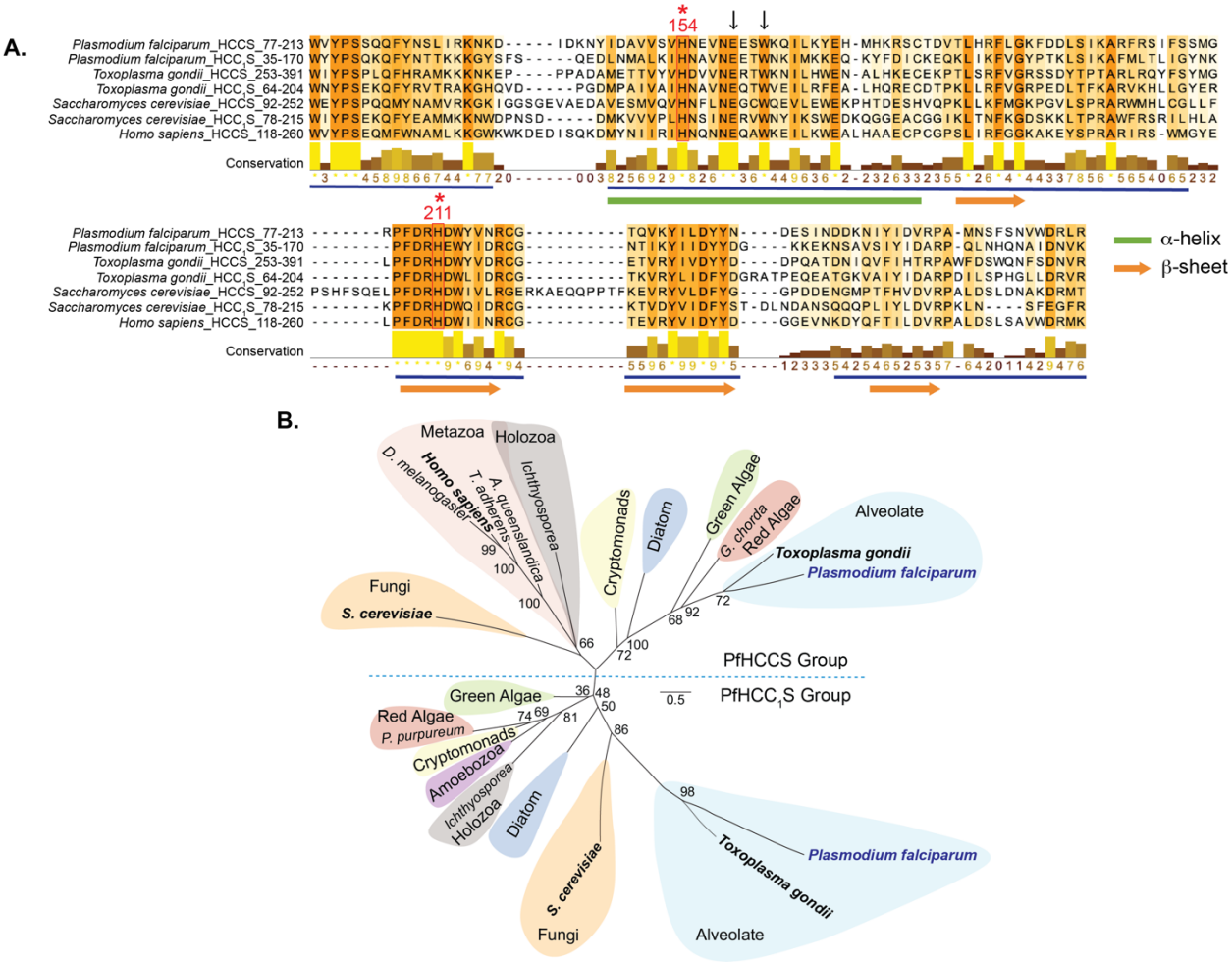

Figure 2. Sequence analysis of HCCS homologs. (A) CLUSTAL Sequence alignment of *P. falciparum* HCCS (77-213) and HCC_1S (35-170) with homologs from *T. gondii* (HCCS: TGME49_293390, 92-252, and HCC_1S: TGME49_314042, 64-204), *S. cerevisiae* (HCCS: CYC3/YAL039C, 92-252; and HCC_1S: CYT2/YKL087C, 78-215), and *H. sapiens* (NP_001116080.1, 118-260). Conservation was measured by JalView with high scores (>5) underlined in blue. Vertical arrows and red asterisks highlight key conserved residues. For simplicity, N-terminal leader sequences are not shown. Residues included in alignments are indicated. (B) Molecular phylogeny of *P. falciparum* HCCS and HCC_1S. BLAST analysis was used to identify orthologs of *P. falciparum* HCCS and HCC_1S, with alignment of 52 sequences (Table S1) for construction of a Maximum Likelihood phylogenetic tree using the IQ-TREE and FigTree software. Bootstrap values are indicated at branch points. The scale bar corresponds to the expected sequence changes per 100 residues.

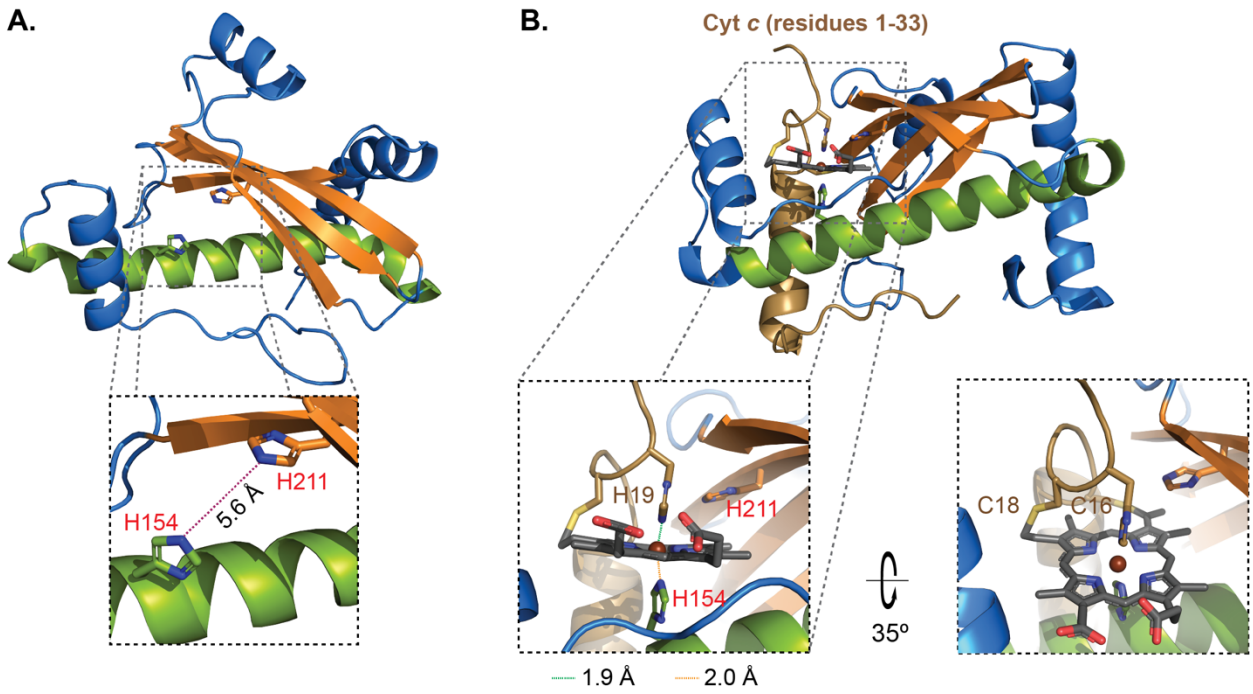

Figure 3. Structural modeling of HCCS. (A) AlphaFold model for PfHCCS showing proximity of conserved active-site His residues (H154, green; and H211, orange; human numbering). (B) AlphaFold 3 model of PfHCCS bound to heme and the N-terminal 33 amino acids of *P. falciparum* cyt *c* (Pf3D7_1404100) showing proximity of conserved His residues from HCCS (H154, green) and cyt *c* (H19, brown), using human sequence numbering.

HCC_1S is essential for parasite viability, ETC function, and cyt c_1 biogenesis. Prior genome-wide and targeted knockout studies in *P. falciparum* and *P. berghei* reported that both HCCS and HCC_1S genes were refractory to disruption and thus likely essential [29-31], but neither protein has been directly studied in *Plasmodium falciparum*. We first focused on HCC_1S, since our prior heterologous expression studies in *E. coli* suggested that this protein does not hemylate cyt *c* but were unable to specify a function for this protein in cyt c_1 biogenesis [17]. To directly test HCC_1S function in *P. falciparum*, we used CRISPR/Cas9 to edit the HCC_1S gene in Dd2 parasites to encode a C-terminal HA-FLAG epitope tag fusion and the 10x aptamer/TetR-DOZI system for conditional protein expression [37]. In this system, protein expression occurs in the presence of the

non-toxic small molecule, anhydrotetracycline (aTc) but is repressed upon aTc washout. PCR analysis confirmed correct editing of the HCC_1S gene in transfected parasites (**Fig. S3, A and B**).

To evaluate HCC_1S expression and its down-regulation upon aTc washout, we performed western blot (WB) experiments to detect the HA-FLAG epitope tags. In repeated experiments that included mitochondrial isolations, we were unable to detect the endogenously tagged protein, likely reflecting very low expression in blood-stage parasites and/or unusual solubility properties that resisted extraction in Triton X-100, SDS, and other detergents. To bypass this limitation, we used reverse transcription and quantitative PCR (RT-qPCR) to measure mRNA levels as a proxy for protein expression. The aptamer/TetR-DOZI system was designed to suppress translation by sequestering transcripts in P-bodies [37], and multiple prior studies have revealed a loss of transcript levels in –aTc conditions that suggests transcript degradation [38, 39]. By RT-qPCR, we detected a strong reduction in transcript levels (~70%) in -aTc compared to +aTc conditions that indicated robust down-regulation of HCC_1S expression upon aTc washout (**Fig. 4A**). This downregulation in -aTc conditions was not observed for HCCS (which was not tagged for knockdown in this line), which instead displayed a modest increase in mRNA levels. To evaluate the impact of HCC_1S knockdown on parasite growth, we synchronized the tagged parasites and evaluated their growth over 6 days (3 intraerythrocytic cycles) in ±aTc conditions. Parasites grew normally +aTc, but their growth was strongly suppressed after 3 days in -aTc conditions (**Fig. 4A**). By blood smear, we detected wide-spread evidence of parasite death at longer growth times (**Fig. S4A**), indicating that HCC_1S function was essential for blood-stage growth.

Prior works have shown that blood-stage parasites can be rescued from defects in the mitochondrial electron transport chain by exogenous addition of the soluble ubiquinone analog, decyl-ubiquinone (dQ) [15-17]. HCC_1S knockdown is predicted to impair biogenesis of cyt c_1, which

is an integral and essential component of ETC Complex III. We thus predicted that dQ might rescue parasites from lethal loss of HCC_1S (**Fig. 1**). To test this prediction, we supplemented parasite cultures with 15 μM dQ and monitored growth over 8 days ±aTc. We observed that dQ supplementation substantially rescued parasite growth in -aTc conditions (**Fig. 4B** and **Fig. S4C**), supporting a key role for HCC_1S in ETC function. Addition of 1 μM proguanil (PRG), which inhibits the secondary pathway for mitochondrial polarization [10, 18], minimally impacted parasite growth in +aTc conditions (**Fig. S4B**) but negated dQ rescue and strongly impaired parasite growth in -aTc/+dQ conditions, as expected for defective ETC function upon HCC_1S knockdown (**Fig. 4B**). Fluorescence microscopy of parasites grown for 5 days ±aTc/+dQ revealed that 1 μM proguanil specifically resulted in dispersed MitoTracker Red staining in -aTc conditions, which indicates mitochondrial depolarization (**Fig. 4C** and **Fig. S5**) [10, 16, 17]. We conclude that HCC_1S knockdown selectively impairs ETC function and sensitizes parasites to mitochondrial depolarization by proguanil, as expected for defective cyt c_1 function.

Impairment of cyt c_1 hemylation may reduce the folding stability and thus detectable levels of cyt c_1 and/or its assembly into Complex III. To test the impact of HCC_1S knockdown on cyt c_1 levels, we tagged the HCC_1S gene with the aptamer/TetR-DOZI system in Dd2 parasites that episomally expressed cyt c_1-GFP [16] and confirmed integration by PCR (**Fig. S6, A and B**). Growth assays with synchronized parasites revealed a strong growth impairment in -aTc conditions (**Fig. S7**) that was very similar to the original HCC_1S knockdown line (**Fig. 4A**). We harvested biological triplicate samples after 3 days of growth in ±aTc/+dQ conditions and fractionated samples by SDS-PAGE followed by western blot (WB) analysis of cyt c_1-GFP, which migrates at ~55 kDa due to N-terminal processing upon mitochondrial import [16] that is similar to prior observations for yeast and human cyt c_1 [40, 41]. This experiment revealed that HCC_1S knockdown

reduced cyt c_1-GFP levels by ~60% but did not impact mitochondrial Hsp60 levels (**Fig. 4D, Fig. S8,** and **Fig. S9**), supporting a key role for HCC_1S in cyt c_1 maturation and stability. It is possible that the GFP tag may enhance the stability of apo cyt c_1 and thus mask a stronger reduction in cyt c_1 levels upon HCC_1S knockdown that would be observed in the absence of the GFP tag. Indeed, N- or C-terminal tags are commonly used to enhance the solubility and/or stability of fusion proteins during recombinant expression [42, 43].

To test the impact of HCC_1S knockdown on cyt c_1 incorporation into Complex III, we harvested samples after 5 days of growth in ±aTc/+dQ conditions and fractionated them by blue-native PAGE followed by WB analysis. Anti-GFP staining revealed a strong band at ~700 kDa in +aTc conditions (**Fig. 4E**, **Fig. S8,** and **Fig. S9**), which is the expected size for Complex III dimer and consistent with recent BN-PAGE detections of Complex III in *P. falciparum* and *Toxoplasma gondii* [44-47]. HCC_1S knockdown in -aTc conditions, however, reduced the intensity of the 700 kDa band by ≥65%, suggesting a substantial defect in cyt c_1 assembly into Complex III. We conclude that HCC_1S function is critical for cyt c_1 biogenesis and assembly into ETC Complex III.

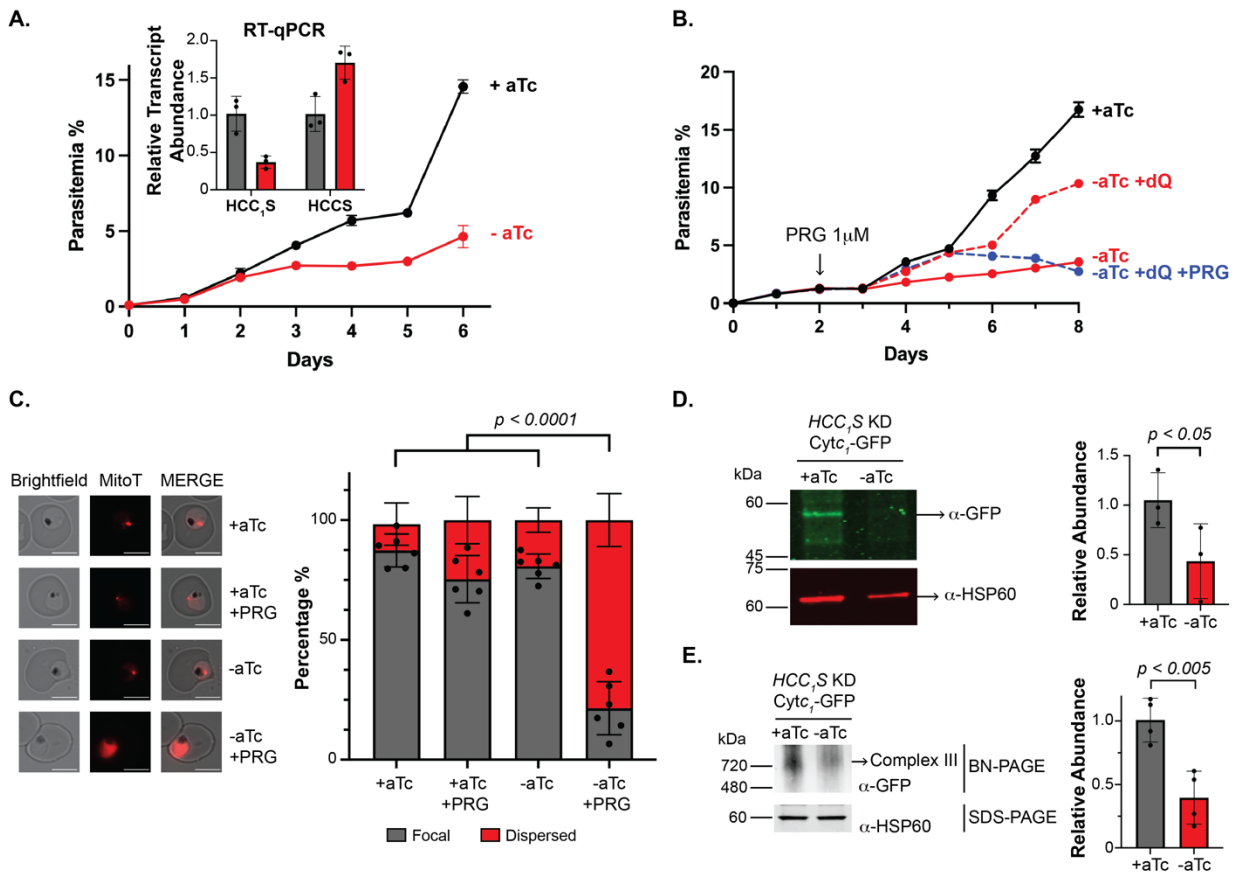

Figure 4. Functional impacts of HCC_1S knockdown. (A) Synchronous growth assay of Dd2 parasites tagged with the aptamer/TetR-DOZI cassette with normal expression (+aTc) or inducible knockdown (-aTc) of HCC_1S expression. Inset: RT-qPCR analysis of HCC_1S and HCCS transcript levels (normalized to I5P, Pf3D7_0802500, and ADSL, Pf3D7_0206700) in biological triplicate samples cultured 4 days ±aTc in 15 μM decyl-ubiquinone (dQ). (B) Synchronous growth assay of HCC_1S knockdown parasites cultured ±aTc, ±15 μM dQ, and ±1 μM proguanil (PRG, added day 2). Data points are the average ±SD of biological triplicates. Statistical analysis of growth differences is shown in Fig. S4C. (C) Fluorescence microscopy images of live HCC_1S knockdown parasites cultured 5 days in 15 μM dQ, ±aTc, and ±1 μM proguanil and stained with 1 nM MitoTracker Red (MitoT). Scale bars represent 5 μm. Thirty parasites were imaged in each of 6 biological replicates to score MitoT staining as focal or dispersed and calculate the percentage of the total population in each condition with the indicated mitochondrial phenotype (average ±SD, *p* value from two-way ANOVA). (D) SDS-PAGE/WB analysis of cyt c_1-GFP expression levels in HCC_1S knockdown parasites cultured 3 days ±aTc/+dQ. Blot was probed with α-GFP and α-Hsp60 antibodies. Band intensities were quantified by densitometry, and the average normalized GFP:Hsp60 signal ±SD based on biological triplicate samples was plotted for ±aTc conditions (*p* value from two-tailed unpaired *t*-test). (E) Blue native-PAGE/WB analysis of cyt c_1-GFP and SDS-PAGE/WB analysis of HSP60 expression levels in HCC_1S knockdown parasites cultured 5 days ±aTc/+dQ. 20 μg of total protein from mitochondrial lysates were loaded for each lane. Blots were probed with α-GFP or α-HSP60 antibodies, with band intensities quantified by densitometry. The average normalized GFP intensity ±SD from biological replicates was plotted for ±aTc conditions.

WB images from biological replicates and uncropped blots for (D) and (E) are shown in **Fig. S8** and **Fig. S9**, respectively.

Loss of HCCS sensitizes parasites to mitochondrial depolarization by proguanil. To directly test HCCS function in blood-stage *P. falciparum*, we used a similar CRISPR/Cas9 strategy to tag the HCCS gene in Dd2 parasites to encode a HA-FLAG fusion tag and the aptamer/TetR-DOZI system for conditional knockdown. We used genomic PCR to confirm successful integration and gene editing in clonal parasites (**Fig. S3, A and C**). As with HCC_1S, we were unable to detect the HA-FLAG-tagged HCCS by WB analysis, suggesting similar low expression. However, RT-qPCR analysis of transcript levels after 3 days of synchronous growth ±aTc revealed a specific ~70% reduction in HCCS mRNA levels (**Fig. 5A**) that was similar to that observed for down-regulation of HCC_1S (**Fig. 4A**). Synchronous growth assays in ±aTc conditions revealed a modest growth defect in -aTc conditions in the third cycle that was less severe than observed for HCC_1S but suggested possible defects in ETC function. To test if this more modest phenotype was specific to HCCS knockdown in Dd2, we also tagged HCCS for knockdown in NF54 parasites and observed a similar phenotype (**Fig. S10**).

Addition of 1 μM proguanil had little or no impact on parasite growth +aTc but resulted in a stringent growth defect and parasite death in -aTc conditions (**Fig. 5B**). This observation suggests that HCCS knockdown results in a critical defect in proton translocation by Complex III and/or IV that is only unmasked in the presence of proguanil and inhibition of the secondary mechanism for mitochondrial polarization. Analysis by fluorescence microscopy, which revealed that proguanil selectively impaired mitochondrial accumulation of MitoTracker Red in -aTc conditions (**Fig. 5C** and **Fig. S5**), provided further support for this conclusion. Based on our prior observation that *P. falciparum* HCCS hemylates cyt *c* in heterologous expression studies in *E. coli* [17], we propose that

HCCS knockdown in parasites impairs holo-cyt *c* biogenesis and reduces proton pumping by ETC Complex III and/or IV that sensitizes parasites to lethal mitochondrial depolarization by proguanil (**Fig. 1**). We further explore the phenotypic differences between HCC_1S and HCCS knockdowns in the Discussion section below.

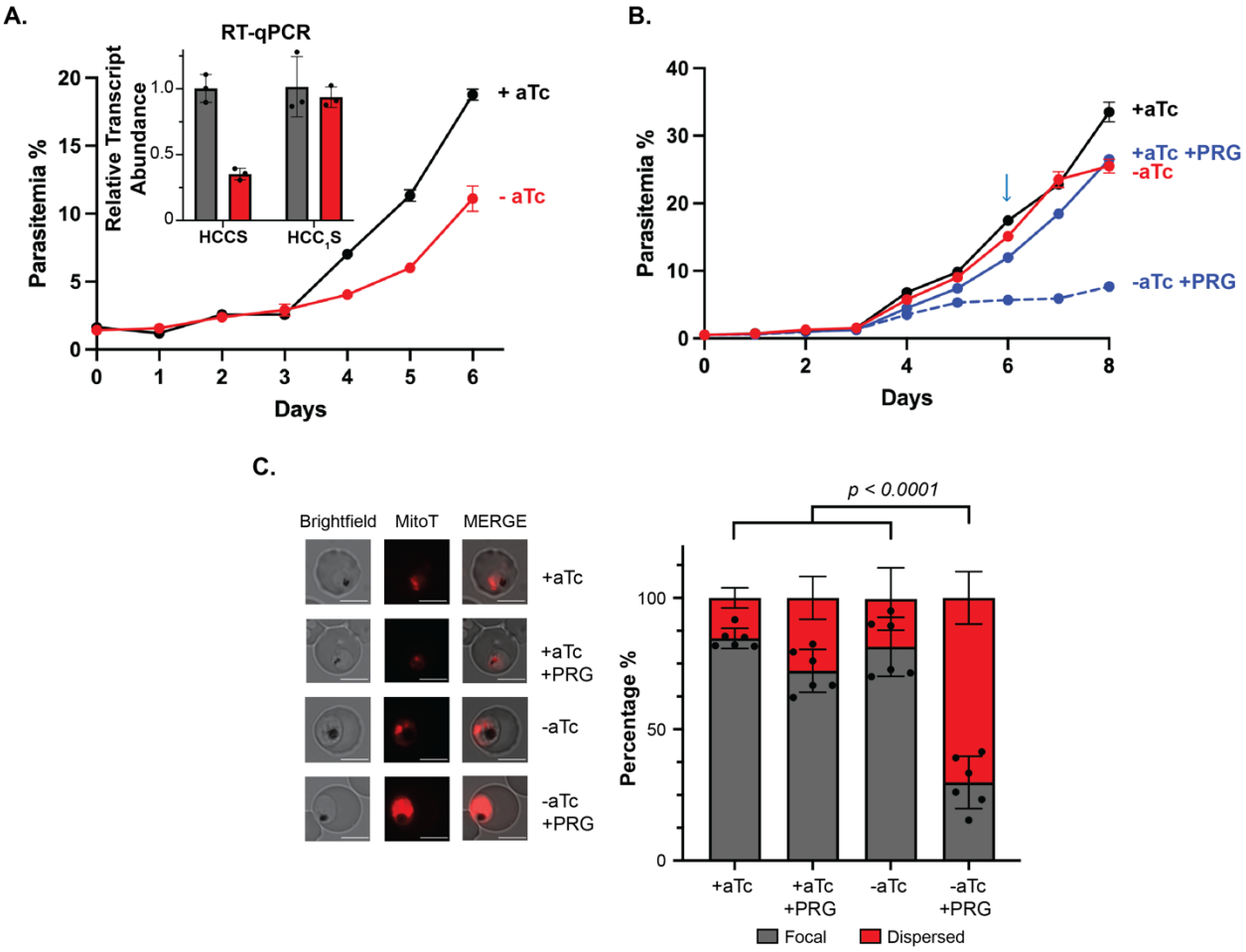

Figure 5. Functional impacts of HCCS knockdown. (A) Synchronous growth assay of Dd2 parasites (clone 1P10) tagged with the aptamer/TetR-DOZI cassette with normal expression (+aTc) or inducible knockdown (-aTc) of HCCS expression. Inset: RT-qPCR analysis of HCCS transcript levels (normalized to I5P and ADSL) in biological triplicates of synchronous parasites cultured 4 days ±aTc. (B) Synchronous growth assay of HCCS knockdown parasites cultured ±aTc and ±1 μM proguanil (PRG). All growth assay data points are the average ±SD of biological triplicates. Arrow indicates culture splits. (C) Fluorescence microscopy images of live HCCS knockdown parasites cultured 5 days ±aTc and ±1 μM proguanil and stained with 1 nM MitoTracker Red (MitoT). Thirty parasites were imaged in each of 6 biological replicates to score

MitoT staining as focal or dispersed and calculate the percentage of the total population in each condition displaying the indicated mitochondrial phenotype (average ±SD). Significance was analyzed by two-way ANOVA to determine the indicated *p* values.

***P. falciparum* HCCS and HCC$_1$S have distinct functional specificities.** Targeted gene knockout studies in *P. berghei* [31], prior biochemical experiments [17], and our observations in this study of parasite growth defects upon individual knockdown of HCC$_1$S or HCCS (exacerbated by non-lethal proguanil) suggest essential and non-redundant functions and specificities for these proteins. To further test this conclusion and if over-expression of HCCS or HCC$_1$S could rescue parasites from knockdown of either endogenous protein, we tagged the HCCS or HCC$_1$S gene for conditional knockdown in the prior Dd2 parasite lines that episomally expressed HCCS-GFP or HCC$_1$S-GFP [17] and confirmed correct integration by genomic PCR (**Fig. S6 and Fig. S11**). Synchronous growth assays revealed that parasites episomally expressing HCC$_1$S-GFP were insensitive to knockdown of endogenous HCC$_1$S and grew similarly in ±aTc conditions (**Fig. 6A**), as expected if episomal HCC$_1$S-GFP functionally replaced the endogenous HCC$_1$S. However, parasites episomally expressing HCCS-GFP displayed a severe growth defect upon HCC$_1$S knockdown in -aTc conditions that was rescued by dQ (**Fig. 6B**), suggesting that HCCS is unable to functionally replace HCC$_1$S. We observed the opposite pattern of rescue for loss of HCCS. Knockdown of endogenous HCCS resulted in no detectable growth impairment in parasites expressing HCCS-GFP (**Fig. 6C**) but a measurable growth defect in parasites expressing HCC$_1$S-GFP (**Fig. 6D)** These observations support our conclusion that HCCS and HCC$_1$S have distinct specificities for hemylation of cyt *c* and c_1 that underpin non-redundant and critical functions.

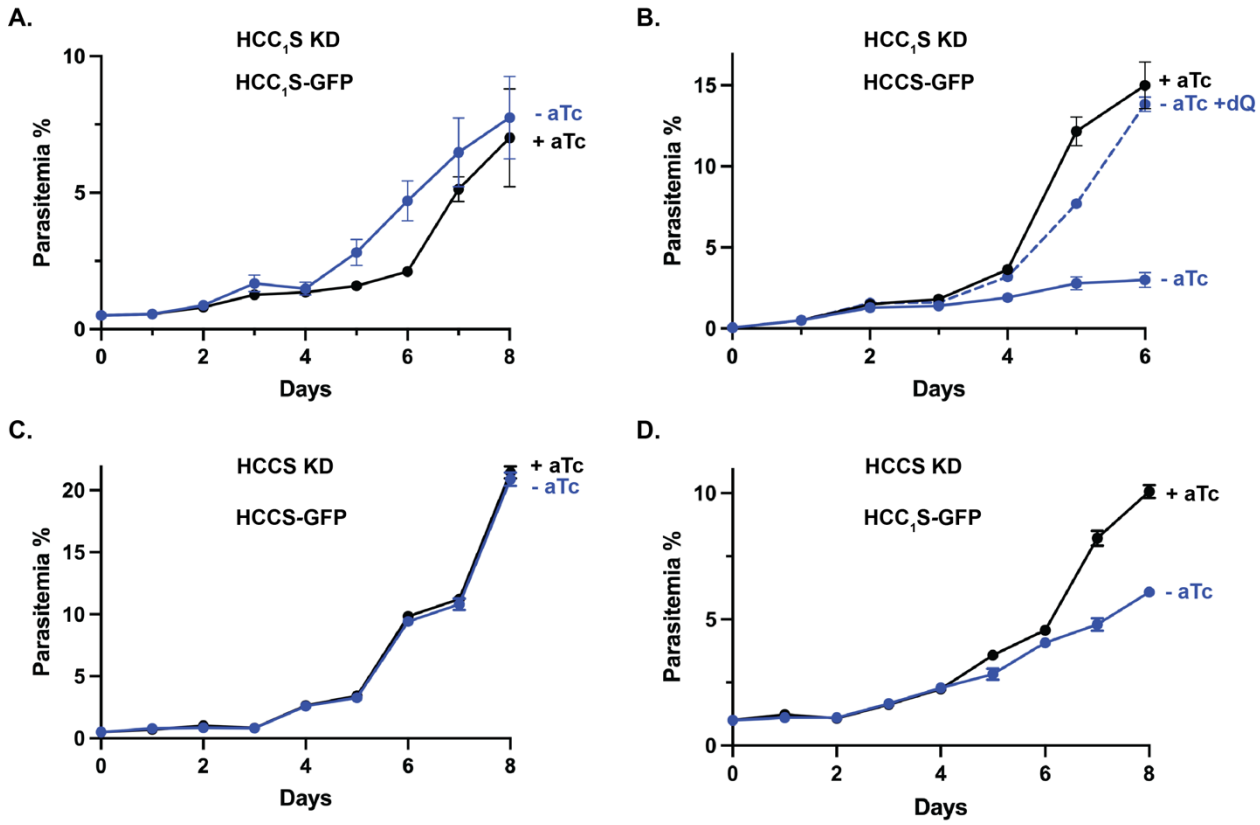

Figure 6. *P. falciparum* HCCS and HCC_1S have non-redundant functions. Synchronous growth assays of HCC_1S knockdown parasites episomally expressing HCC_1S-GFP (A) or HCCS-GFP (B) or HCCS knockdown parasites episomally expressing HCCS-GFP (C) or HCC_1S-GFP (D) and cultured in ±aTc and ±dQ (15 µM) conditions. All growth assay data points are the average ±SD of biological triplicate samples.

DISCUSSION

The maturation and function of heme-bound cyt *c* and cyt c_1 are central to mitochondrial electron transport chain activity in malaria parasites, especially respiratory Complexes III and IV (**Fig. 1**). Complex III is the molecular target of atovaquone [9] and has received considerable attention in the discovery and development of new antimalarial drugs [11, 13], especially as parasites that harbor atovaquone-resistant mutations are unable to complete mosquito-stage development and transmit to new hosts [48, 49]. Prior work has also highlighted effective strategies to target parasites via Complex III during mosquito infection [12]. These studies are nearly all based on targeting cyt *b* of Complex III, and few strategies have been identified to interfere with other essential ETC factors and functions. Recent efforts dissected the essential roles of cyt *c* and c_1 for parasite ETC activity [17], but it is unclear how these protein functions might be directly targeted. In the present work, we identified critical independent functions for HCCS and HCC_1S, required for covalent attachment of heme to cyt *c* and c_1. This work lays a foundation for deeper structural and mechanistic studies to unravel differences within the heme-binding pockets of the human and parasite HCCS enzymes that can underpin selective therapeutic targeting of the *P. falciparum* ETC.

Functional differences between *P. falciparum* HCCS and HCC_1S. This study, in combination with prior functional tests based on heterologous reconstitution in *E. coli* [17], unveiled separate key functions for parasite HCCS and HCC_1S in maturation of cyt *c* and c_1, respectively (**Fig. 7**). Knockdown of HCC_1S resulted in impaired cyt c_1 biogenesis and incorporation into Complex III, lethal ETC dysfunction that stringently limited growth and could not be rescued by HCCS over-expression, and strong sensitivity to mitochondrial depolarization in the presence of proguanil. In comparison, HCCS knockdown caused a modest reduction in parasite growth that required

combinatorial treatment with proguanil to stringently kill parasites via mitochondrial depolarization. It remains an important future challenge to define and understand the molecular differences between HCCS and HCC_1S that confer specificity for hemylation of cyt *c* versus cyt c_1. These functional differences may reflect sequence-specific features of each protein that underpin specific binding and/or heme attachment to cyt *c* or cyt c_1. Alternatively, or in addition, there may be other cellular factors that interact with HCCS and HCC_1S that contribute to substrate specificity.

The strong growth defect due to loss of HCC_1S phenocopies direct knockdown of cyt c_1 [17] and underscores the tight dependence of ETC function and parasite viability on cyt c_1 expression and heme-dependent maturation. This stringent coupling to cyt c_1 may reflect both the direct function of cyt c_1 in mediating critical electron transfer from the Rieske Fe-S protein to cyt *c* [50] and a secondary structural role played by cyt c_1 in the assembly and integrity of Complex III [51], both of which are likely impaired by loss of HCC_1S (**Fig. 7**). Indeed, our data provide direct evidence that HCC_1S knockdown results in defective cyt c_1 incorporation into Complex III (**Fig. 4E**). Prior work in yeast also highlighted that hemylation of cyt c_1 by HCC_1S is coupled to mitochondrial import and N-terminal processing [40]. Import and processing of cyt c_1 is sparsely studied in apicomplexan parasites. Nevertheless, recent work in *Toxoplasma* identified that the cyt c_1 leader sequence that is cleaved upon mitochondrial import is incorporated into ATP synthase as a stable structural sub-unit [45, 52]. It is not clear if this sub-unit is required for assembly and/or function of ATP synthase nor if this feature is conserved in *Plasmodium* parasites. Proteomic profiling of ATP synthase composition in *P. falciparum* did not report this cyt c_1-derived subunit [44], although associations between cyt c_1 and ATP synthase have been detected in blood-stage parasites [53]. Nevertheless, this observation in *T. gondii* suggests an additional (and elegant)

biochemical mechanism to couple cyt c_1 import, hemylation, and maturation in apicomplexan parasites to broader assembly and function of the mitochondrial ETC and ATP synthase.

The more modest growth phenotype upon knockdown of HCCS compared to HCC_1S, despite similar reductions in transcript abundance, is somewhat puzzling and may have multiple underpinnings. Cyt *c* function, which depends on heme attachment, is essential for ETC function and parasite viability [17]. The mild phenotype for HCCS knockdown thus contrasts with the lethal phenotype for cyt *c* knockdown, the strong expectation of HCCS essentiality based on prior knockout studies [29-31], and the selective ability of HCCS (and not HCC_1S) to hemylate cyt *c* in heterologous studies in *E. coli* [17]. The first explanation we considered is that HCCS knockdown was insufficiently stringent such that residual expression was enough to support cyt *c* hemylation and attenuate the phenotypic severity of partial knockdown. However, HCCS knockdown sensitizes parasites to a much stronger, lethal phenotype when combined with 1 μM proguanil. This observation suggests a critical defect in proton pumping by Complexes III and/or IV due to HCCS knockdown, despite modest growth inhibition by itself, which can explain the synergistic lethality with proguanil which blocks the secondary pathway for mitochondrial polarization (**Figs. 1 and 7**).

Based on these observations, we favor an alternative model that HCCS knockdown in our current system impairs cyt *c* hemylation sufficiently to interfere with electron transport between Complexes III and IV but without substantially impairing oxidative recycling of ubiquinone by Complex III. A corollary of this model is that cyt *c*-mediated electron transport to Complex IV and concomitant proton pumping may be more tightly coupled to cyt *c* function than ubiquinone recycling by Complex III. This model predicts that a more stringent knockdown of HCCS, which might be achieved by adding a 5' aptamer to the current 10x aptamers on the 3' end of the HCCS

gene, will impair ubiquinone recycling and result in a lethal growth phenotype that matches direct knockdown of cyt *c* and can be rescued by decyl-ubiquinone [17]. We are currently testing this prediction.

Implications for evolution of *P. falciparum* HCCS and HCC_1S. Cyt *c* and c_1 are retained by nearly all aerobic eukaryotes with a mitochondrion [21, 22, 54]. Nature has evolved at least three distinct biochemical systems for *c*-type cytochrome hemylation, two of which are multi-protein systems that are unrelated evolutionarily to the single-protein HCCS system [19, 20, 55]. HCCS and/or HCC_1S proteins are broadly present in eukaryotes, including opisthokonts, alveolates, and amoebozoa [55]. This broad retention across phylogenetically divergent organisms suggests that separate HCCS and HCC_1S enzymes are ancient features of many eukaryotes. Within these clades that contain an HCCS homolog, metazoa and amoebozoa retain a single homolog (**Fig. 2B**) that appears to bifunctionally hemylate both cyt *c* and c_1 [20, 26]. For these organisms, low-level promiscuous hemylation of cyt c_1 (in addition to the cognate cyt *c* substrate) was presumably enhanced in an ancestral organism such that a separate HCC_1S enzyme became redundant and was lost [20, 24]. Evidence for this model is provided by yeast, in which HCCS hemylates cyt *c* and less efficiently cyt c_1 [26]. As previously noted [55], the evolutionary origin of HCCS is unclear and remains a future challenge to understand. Indeed, our structural similarity searches of the RCSB Protein Data Bank with the AlphaFold-predicted *P. falciparum* HCCS structure using the Dali server [56] failed to identify substantial similarity to known protein structures.

Our results and those from prior biochemical [17] and gene-disruption studies [29-31] support a model in which both *P. falciparum* HCCS and HCC_1S serve functionally independent and essential roles. This scenario contrasts with the related apicomplexan parasite *Toxoplasma gondii*, in which only the HCCS homolog appears to be essential for tachyzoite survival and shows evidence of

hemylating both cyt *c* and c_1, despite retention of an HCC_1S paralog [28]. Thus, the function, retention, and essentiality of HCCS and HCC_1S homologs may be idiosyncratically tuned during evolution of different organisms depending on their unique cellular pressures for growth and survival. These functional differences may also involve additional cellular factors that influence observed specificities in vivo. Broader and deeper functional studies of these enzymes in differing organisms will facilitate understanding of the gain and loss of activities that underpin evolution of this enzymatic activity central to eukaryotic respiration.

Source of heme for HCCS and HCC_1S. *Plasmodium* parasites require heme as a metabolic cofactor for incorporation into mitochondrial cytochromes *b* and c_1 in Complex III, cyt *c*, and cytochrome a/a_3 in Complex IV [3-5]. Parasites retain a complete biosynthesis pathway to make heme in the mitochondrion, but this pathway is dispensable for parasites during blood-stage growth and is only required during mosquito- and liver-stage growth [57-62]. This observation implies that parasites can scavenge host-derived heme, although possible mechanisms for mobilizing labile heme released in the food vacuole during hemoglobin digestion and trafficking it to the mitochondrion remain undefined. HCCS and HCC_1S function on the outer leaflet of the mitochondrial inner membrane [63] and must bind heme for subsequent attachment to cyt *c* and c_1. Although proteomic studies in human cells suggest that the terminal heme synthesis enzyme, ferrochelatase, associates with other heme metabolism proteins at the mitochondrial inner membrane that may include or facilitate heme acquisition by HCCS [64, 65], parasite mechanisms for acquisition of biosynthetic or scavenged heme by HCCS and HCC_1S are unknown. Our current study does not provide an answer to this question but lays a foundation for defining key interactions by these enzymes in *P. falciparum*, either through immunoprecipitation or proximity biotinylation

coupled to tandem mass spectrometry, that can illuminate the heme-trafficking pathways that support biogenesis of heme-bound cyt *c* and c_1.

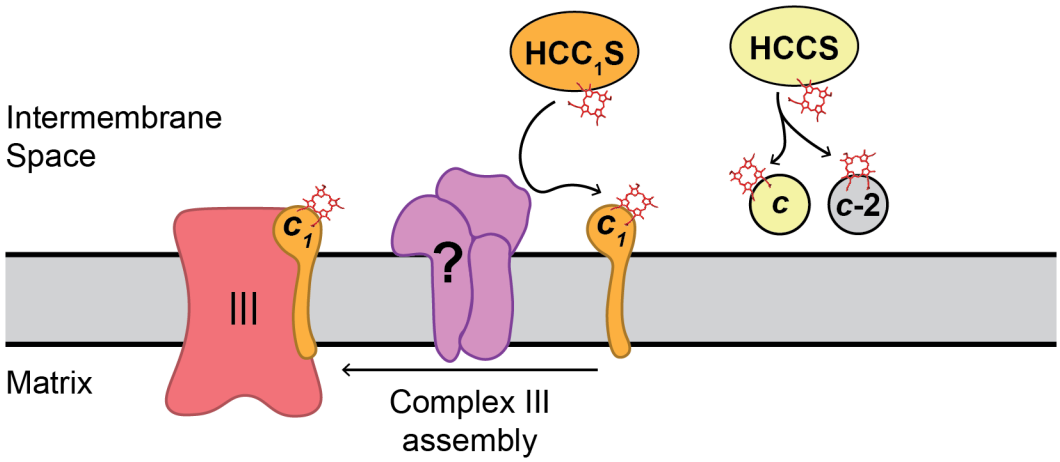

Figure 7. Schematic model for functional specificities of *P. falciparum* HCCS and HCC_1S. The question mark indicates uncertainty in the mechanism of cyt c_1 assembly into Complex III.

METHODS

Cloning. Creation of pTEOE plasmids encoding HCCS-GFP and HCC_1S-GFP was previously described [17]. To tag HCCS and HCC_1S for inducible knockdown, guide RNA sequences corresponding to TAACAAAAATTGTGAAAAAT and GCAAATGTGCAACAAACAAT (HCCS) and TTATTTATATAAAGATTTGT (HCC_1S) were cloned into the pAIO CRISPR/Cas9 vector [66] using ligation-independent methods (primers HCCSgRNA1F, HCCSgRNA1R, HCCSgRNA2F, HCCSgRNA2R, HCC1SgRNA1F and HCC1SgRNA1R) by the Mutation Generation & Detection Core at the University of Utah. Donor repair plasmids for each gene were creating using assembly PCR to create a fused sequence containing a 3' UTR homology region (HR) separated by an AflII site from a 5' homology region that contained the 3' end of the coding sequence (without stop codon) for each gene. This fused insert was then cloned into the pMG75 [37] plasmid using AscI/AatII cloning sites and ligation-independent methods and confirmed by Sanger sequencing. Donor plasmids to tag each gene were cloned from genomic DNA using the following primer sets: HCCS (3' HR: primers 51/52, 5' HR: primers 53/54) and HCC_1S (3' HR: primers 55/56, 5' HR: primers 57/58). Primer sequences are given in Table S2.

Parasite Culturing and Transfection. Experiments in this study were performed using *Plasmodium falciparum* Dd2 [67] and NF54 [68] parasites, whose identities were confirmed based on expected drug sensitivities and resistance. Parasites were *Mycoplasma*-free by PCR test. Dd2 parasites stably transfected with a pTEOE episome [62] encoding HCCS-GFP or HCC_1S-GFP were available from a previously reported study [17] and cultured in 5 nM WR99210.

Parasites were cultured as previously described [17, 39], using Roswell Park Memorial Institute medium (RPMI-1640, Thermo Fisher 23400021) supplemented with 2.5 g/L AlbuMAX I Lipid-Rich BSA (Thermo Fisher 11020039), 15 mg/L hypoxanthine (Sigma H9636), 110 mg/L

sodium pyruvate (Sigma P5280), 1.19 g/L HEPES (Sigma H4034), 2.52 g/L sodium bicarbonate (Sigma S5761), 2 g/L glucose (Sigma G7021), and 10 mg/L gentamicin (Invitrogen 15750060). Parasites were grown at 2% hematocrit in human red blood cells obtained from the University of Utah Hospital blood bank, at 37˚C, and at 5% O_2, 5% CO_2, and 90% N_2. Parasite-infected cultures were transfected in 1x cytomix [69] containing 50-100 µg midi-prep DNA by electroporation in 0.2 cm cuvettes using a Bio-Rad Gene Pulser Xcell system (0.31 kV, 925 µF). Transgenic parasites were selected based on plasmid resistance (blasticidin-S-deaminase) to 6 µM blasticidin-S (Gold Biotechnology B-800-100). Transgenic parasites modified with the aptamer/TetR-DOZI system or pTEOE episomes were cultured in 0.5-1 µM anhydrotetracycline (aTc, Cayman Chemicals 10009542) or 5 nM WR99210 (Jacobus Pharmaceuticals), respectively. Genetically modified parasites were genotyped by PCR. For growth assays with decyl-ubiquinone (dQ, Caymen Chemicals 55486005) and/or proguanil (Sigma 637321), the growth medium was supplemented with 15 µM dQ (≤0.3 % DMSO) and/or 1 µM proguanil (≤0.3 % DMSO).

For CRISPR/Cas9-based genome-editing experiments to tag HCCS (PF3D7_1224600) and HCC_1S (PF3D7_1203600) to encode a C-terminal HA-FLAG epitope tag and the 10X aptamer/TetR-DOZI system for aTc-dependent expression [37], Dd2 or NF54 parasites were transfected in duplicate with 50 µg each of the linearized pMG74 donor plasmid (with gene-specific homology arms) and pAIO plasmid [66] (encoding Cas9 and gene-specific gRNA). Transfected parasites recovered for 48 hours in drug-free media and then were selected with 0.5 µM aTc and 6 µM blasticidin-S. Polyclonal parasites that returned from transfection were genotyped with primer sets 77_P1/54_P2, 53_P3/83_P4, 77_P1/PfHCCSRv7_P7 and 5'Hsp60Rv1_P8/PfHCCSRv9_P9 (HCCS) and 86_P1/58_P2, 57_P3/83_P4, 86_P1/PfHCC1SRv4_P7 and 5'Hsp60Rv1_P8/PfHCC1SRv4_P9 (HCC_1S) to test for unmodified

locus and successful integration, respectively. Polyclonal parasites that PCR analysis indicated were fully integrated without unmodified locus were used without cloning. Otherwise, clonal parasite integrants were obtained by limiting dilution. The Dd2 lines with HCC_1S tagged for KD at its endogenous locus and episomally expressing cyt c_1-GFP was created by first transfecting Dd2 parasites with cyt c_1-GFP/pTEOE (selection with WR99210) and then transfecting with pAIO CRISPR/Cas9 and pMG74/donor repair plasmids to tag the HCC_1S gene for knockdown (selection with blasticidin-S and aTc). Successful integration was confirmed by genotyping PCR as above. A similar strategy was used to tag HCCS or HCC_1S for KD at its endogenous locus in DD2 parasites that episomally expressed HCCS-GFP or HCC_1S-GFP and were previously reported [17]. Primer sequences are given in Table S2.

Parasite Growth Assays. For synchronous growth assays, asynchronous parasite cultures were treated with 5% D-sorbitol (Sigma S7900) for 10 minutes, resulting in a culture that contained ring-stage parasites. Sorbitol-treated cultures were then washed three times with RPMI media lacking aTc and divided into two equal parts before supplementing one part with 0.5 μM aTc. Parasites were diluted to 0.5% parasitemia ±aTc and allowed to grow over several days with daily media changes in biological triplicate samples. Parasitemia was monitored daily by flow cytometry by diluting 20 μL of each resuspended parasite culture well from each replicate into 200 μL of 1.0 μg/mL acridine orange (Invitrogen A3568) in phosphate buffered saline (PBS) pH 7.5 and analysis on a BD FACSCelesta system monitoring SSC-A, FSC-A, PE-A, FITC-A and PerCP-Cy5-5A channels. Parasitemia values are the average ± standard deviation of biological replicates. Growth assays in which parasitemia was plotted versus 2-day growth cycle was analyzed with an exponential growth model using GraphPad Prism 9.0. Observed differences in rate constants for

exponential growth in different conditions were analyzed for significance by ANOVA using GraphPad Prism 9.0.

RT-qPCR Analyses. Biological replicate cultures of HCCS or HCC_1S knockdown Dd2 parasites were synchronized in 5% D sorbitol and grown for 72 hours in +aTc or -aTc/+dQ conditions prior to harvest. Four mL cultures at ~10% parasitemia were harvested by centrifugation (2000 rpm for 3 min in a Beckman Coulter Allegra 25R table-top centrifuge) and stored at -20˚C until use. Total RNA was isolated from frozen pellets and resuspended using a modified Trizol (Invitrogen) extraction protocol, as previously described [39]. Washed and dried RNA pellets were resuspended in RNAse-free water, quantified by NanoDrop Spectrophotometer, and used immediately or stored at -80˚C. One µg of RNA was DNAse-treated and reverse-transcribed using Superscript IV kit (Invitrogen) with the addition of 1 µM gene-specific reverse primers HCCSqR1, HCC_1SqR1, GFPqR1, I5PqR1, and ADSLqR1. Subsequent cDNA was analyzed in technical triplicate through quantitative PCR using SYBR Green fluorescent probe with ROX (Invitrogen) in a QuantStudio 7 qPCR instrument (Applied Biosystems). C_p values for each target gene (primers HCCS_qF1, HCCS_qR1, HCC_1S_qF1, and HCC_1S_qR1) were normalized to average C_p values of the nuclear I5P gene (PF3D7_0802500, I5P_qF1 and I5P_qR1) and ADSL gene (Pf3D7_0206700, ADSL_qF1 and ADSL_qR1), then used to calculate relative RNA abundance values for each culture condition ±aTc, with normalization of the +aTc sample to a value of 1. Data is reported as the average ± SD of ≥3 biological replicates for each condition. All primer sequences are given in Table S2.

Mitochondrial Isolation. Biological replicate 60 mL cultures of HCC_1S KD Dd2 parasites were harvested at 15-18% parasitemia and treated with 0.05% saponin (Sigma 84510) in PBS (pH 7.2), incubated for 5 min at ambient temperature, and centrifuged at 3,000 x *g* for 30 min at 4ºC. Isolated parasite-containing pellets were washed twice with PBS pH 7.2 and stored at -80˚C until use.

Parasite pellets were thawed on ice and resuspended with MEST buffer (20 mM Tris-HCl pH 7.4, 250 mM D-sorbitol, 1 mM EDTA pH 8.0, and EDTA-free protease inhibitor cocktail (Thermo Fisher J61852.XF). Parasites were lysed by 10 passages through a syringe fitted with a 25-gauge needle and 20 passages with a 27-gauge needle. The cellular debris and unlysed parasites were pelleted twice by cold centrifugation at 6,000 x *g* for 10 min at 4ºC. The supernatant was centrifuged 15 min at 17,000 x *g* at 4ºC to recover the crude mitochondrial fraction in the pellet. Total protein from the mitochondrial fraction was quantified using the Lowry method [70].

SDS/Blue-Native PAGE and Western Blot Analyses. To evaluate expression levels of cyt c_1-GFP in the HCC_1S KD line ±aTc, biological replicate cultures of parasites were synchronized with 5% D-sorbitol to rings, grown for 72 hours +aTc or -aTc/+dQ, harvested as second-cycle trophozoites and schizonts, processed as described above to isolate mitochondria, and then analyzed by SDS-PAGE or blue native (BN)-PAGE.

For SDS-PAGE, 50 µg of mitochondrial protein was heated in 1X SDS sample buffer containing 5% fresh β-mercaptoethanol for 5 min at 65˚C and loaded onto 12% polyacrylamide gels, fractionated by gel electrophoresis, and transferred to nitrocellulose membrane, as previously described [16, 17]. Membranes were blocked at room temperature for 1 hour in 5% skim milk/PBS and probed overnight at 4˚C with 1:1000 dilutions of rabbit anti-HSP60 (Novus NBP2-12734) and goat anti-GFP (Antibodies.com A121560) antibodies. Membranes were washed 3 times in TBS buffer supplemented with 0.1% TWEEN-20 (Millipore P1379), probed with 1:5,000 dilutions of donkey anti-rabbit IRDye680 (Licor 926-68023) and donkey anti-goat IRDye800CW (Licor 926-32214) 2˚ antibodies in TBST buffer, washed 3 times in TBST buffer, and imaged on a Licor Odyssey CLx imager. Band intensities were quantified by densitometry using ImageJ and analyzed by GraphPad Prism 9.0.

For BN-PAGE, 20 µg of mitochondrial protein was mixed with 1X Native-PAGE sample buffer (Invitrogen BN2003) supplemented with 1% digitonin and incubated on ice for 15 min. The sample was centrifuged at 17,000 x g for 10 min., and 20 µL of the supernatant was loaded and run on a NativePAGE 4-16% Bis-Tris gel (Invitrogen BN1002BOX) and transferred to PVDF membrane (Rio-Rad 1620177, pre-wetted in 70% methanol). The membrane was destained in 70% methanol and then washed with TBS-T, blocked, probed with goat anti-GFP 1˚ antibody, and washed as above. The membrane was then probed with a 1:5,000 dilution of rabbit anti-goat-HRP 2˚ antibody (Santa Cruz Biotechnology sc-2768), washed, developed using the SuperSignal West Pico PLUS enhanced chemiluminescence reagent (Thermo Fisher 34577), and imaged on an Invitrogen/Thermo Fisher iBright 1500 imager.

Fluorescence Microscopy. For mitochondrial depolarization experiments with HCCS and HCC_1S knockdown parasites, cultures were synchronized with 5% D-sorbitol, cultured +aTc or -aTc/+dQ for 120 hours before addition of 1 µM proguanil for 4 hours and 1 nM MitoTracker Red for 30 minutes, and imaged as third-cycle trophozoites/schizonts. 30 total parasites for each condition across 4 independent experiments were scored in a sample-blinded manner for focal or dispersed MitoTracker signal. Images were taken on DIC/brightfield, DAPI, and RFP channels using an EVOS M5000 imaging system. Images were processed using ImageJ with all brightness/contrast adjustments made on a linear scale.

Alignment and Phylogenetic Analyses. The protein sequences for parasite HCCS (Pf3D7_1224600) and HCC_1S (Pf3D7_1203600) were analyzed by PSI-BLAST [71] to identify orthologs in representative species of distinct organisms. Sequences (Table S1) were aligned by CLUSTAL Omega [72] and analyzed using Jalview [73]. The multisequence alignment was uploaded to the IQ-TREE webserver (http://iqtree.cibiv.univie.ac.at) with ultrafast bootstrap analysis [74]. The

resulting maximum likelihood phylogenetic tree from 1000 bootstrap alignments was analyzed using FigTree (http://tree.bio.ed.ac.uk/software/figtree/). The raw phylogenetic tree is shown in **Fig. S12**.

Structural Modeling. Structural models for human HCCS and *P. falciparum* HCCS and HCC_1S were obtained from the AlphaFold Protein Structure Database (https://alphafold.ebi.ac.uk) [75]. Structural models for parasite HCCS bound to heme without or with the N-terminal 33 residues of *P. falciparum* cyt c (PF3D7_1404100) were generated using AlphaFold 3 [34]. Protein models were visualized and analyzed using PyMOL [76].

SUPPORTING INFORMATION. AlphaFold models of HCCS (Figure S1), sequence conservation and conformational variation of HCCS (Figure S2), genome editing of HCC_1S and HCCS in parasites (Figure S3), growth analysis of HCC_1S knockdown parasites (Figure S4), additional live-parasite microscopy images of HCC_1S and HCCS knockdown parasites cultured ±proguanil (Figure S5), genome editing of HCC_1S in parasites transfected for episomal expression (Figure S6), growth assay of HCC_1S knockdown parasites transfected for episomal expression of cyt c_1-GFP (Figure S7), additional western blot images of HCC_1S knockdown parasites episomally expressing cyt c_1-GFP (Figure S8), uncropped western blot images (Figure S9), genotyping HCCS integration in NF54 parasites (Figure S10), genotyping HCCS integrations in parasites transfected for episomal expression (Figure S11), raw phylogenetic tree of HCCS and HCC_1S homologs (Figure S12), list of organisms and HCCS or HCC_1S protein sequences aligned in Figure S12 (Table S1), list of primers (Table S2) (PDF)

ACKNOWLEDGMENTS. We thank Chris Hill, Robert Kranz, Tyler Starr, Henry Wienkers, Dennis Winge and members of the Sigala lab for helpful discussions. We thank Megan Okada for illustration assistance in making the scheme in Fig. 1. This work was supported by NIH grant R35GM133764 (PAS) and a Burroughs Wellcome Fund Career Award at the Scientific Interface (PAS). PAS is a Pew Biomedical Scholar, supported by The Pew Charitable Trusts. DNA synthesis and sequencing, fluorescence microscopy, creation of CRISPR/Cas9 reagents, and flow cytometry were performed using core facilities at the University of Utah and the Center for Iron and Heme Disorders.

REFERENCES

(1) WHO. *World Malaria Report*; Geneva, Switzerland, 2023.

(2) D'Alessandro, A.; Dzieciatkowska, M.; Nemkov, T.; Hansen, K. C. Red blood cell proteomics update: is there more to discover? *Blood Transfus* **2017**, *15*, 182-187.

(3) Sigala, P. A.; Goldberg, D. E. The peculiarities and paradoxes of *Plasmodium* heme metabolism. *Annu. Rev. Microbiol.* **2014**, *68*, 259-278.

(4) van Dooren, G. G.; Kennedy, A. T.; McFadden, G. I. The use and abuse of heme in apicomplexan parasites. *Antioxid. Redox Signal.* **2012**, *17*, 634-656.

(5) Kloehn, J.; Harding, C. R.; Soldati-Favre, D. Supply and demand-heme synthesis, salvage and utilization by Apicomplexa. *FEBS J.* **2021**, *288*, 382-404.

(6) Francis, S. E.; Sullivan, D. J., Jr.; Goldberg, D. E. Hemoglobin metabolism in the malaria parasite *Plasmodium falciparum*. *Annu. Rev. Microbiol.* **1997**, *51*, 97-123.

(7) Blasco, B.; Leroy, D.; Fidock, D. A. Antimalarial drug resistance: linking *Plasmodium falciparum* parasite biology to the clinic. *Nat Med.* **2017**, *23*, 917-928.

(8) Delves, M.; Plouffe, D.; Scheurer, C.; Meister, S.; Wittlin, S.; Winzeler, E. A.; Sinden, R. E.; Leroy, D. The activities of current antimalarial drugs on the life cycle stages of *Plasmodium*: a comparative study with human and rodent parasites. *PLoS Med.* **2012**, *9*, e1001169.

(9) Fry, M.; Pudney, M. Site of action of the antimalarial hydroxynaphthoquinone, 2-[trans-4-(4'-chlorophenyl) cyclohexyl]-3-hydroxy-1,4-naphthoquinone (566C80). *Biochem. Pharmacol.* **1992**, *43*, 1545-1553.

(10) Painter, H. J.; Morrisey, J. M.; Mather, M. W.; Vaidya, A. B. Specific role of mitochondrial electron transport in blood-stage *Plasmodium falciparum*. *Nature* **2007**, *446*, 88-91.

(11) Antonova-Koch, Y.; Meister, S.; Abraham, M.; Luth, M. R.; Ottilie, S.; Lukens, A. K.; Sakata-Kato, T.; Vanaerschot, M.; Owen, E.; Jado, J. C.; Maher, S. P.; Calla, J.; Plouffe, D.; Zhong, Y.; Chen, K.; Chaumeau, V.; Conway, A. J.; McNamara, C. W.; Ibanez, M.; Gagaring, K.; Serrano, F. N.; Eribez, K.; Taggard, C. M.; Cheung, A. L.; Lincoln, C.; Ambachew, B.; Rouillier, M.; Siegel, D.; Nosten, F.; Kyle, D. E.; Gamo, F. J.; Zhou, Y.; Llinas, M.; Fidock, D. A.; Wirth, D. F.; Burrows, J.; Campo, B.; Winzeler, E. A. Open-source discovery of chemical leads for next-generation chemoprotective antimalarials. *Science* **2018**, *362*, eaat9446.

(12) Paton, D. G.; Childs, L. M.; Itoe, M. A.; Holmdahl, I. E.; Buckee, C. O.; Catteruccia, F. Exposing Anopheles mosquitoes to antimalarials blocks *Plasmodium* parasite transmission. *Nature* **2019**, *567*, 239-243.

(13) Nilsen, A.; LaCrue, A. N.; White, K. L.; Forquer, I. P.; Cross, R. M.; Marfurt, J.; Mather, M. W.; Delves, M. J.; Shackleford, D. M.; Saenz, F. E.; Morrisey, J. M.; Steuten, J.; Mutka, T.; Li, Y.; Wirjanata, G.; Ryan, E.; Duffy, S.; Kelly, J. X.; Sebayang, B. F.; Zeeman, A. M.; Noviyanti, R.; Sinden, R. E.; Kocken, C. H. M.; Price, R. N.; Avery, V. M.; Angulo-Barturen, I.; Jimenez-Diaz, M. B.; Ferrer, S.; Herreros, E.; Sanz, L. M.; Gamo, F. J.; Bathurst, I.; Burrows, J. N.; Siegl, P.; Guy, R. K.; Winter, R. W.; Vaidya, A. B.; Charman, S. A.; Kyle, D. E.; Manetsch, R.; Riscoe, M. K. Quinolone-3-diarylethers: a new class of antimalarial drug. *Sci. Transl. Med.* **2013**, *5*, 177ra137.

(14) Simao-Gurge, R. M.; Wunderlich, G.; Cricco, J. A.; Cubillos, E. F. G.; Domenech-Carbo, A.; Cebrian-Torrejon, G.; Almeida, F. G.; Cirulli, B. A.; Katzin, A. M. Biosynthesis of heme O in intraerythrocytic stages of Plasmodium falciparum and potential inhibitors of this pathway. *Sci Rep* **2019**, *9*, 19261.

(15) Ke, H. J.; Morrisey, J. M.; Ganesan, S. M.; Painter, H. J.; Mather, M. W.; Vaidya, A. B. Variation among *Plasmodium falciparum* Strains in Their Reliance on Mitochondrial Electron Transport Chain Function. *Eukaryot. Cell* **2011**, *10*, 1053-1061.

(16) Falekun, S.; Sepulveda, J.; Jami-Alahmadi, Y.; Park, H.; Wohlschlegel, J. A.; Sigala, P. A. Divergent acyl carrier protein decouples mitochondrial Fe-S cluster biogenesis from fatty acid synthesis in malaria parasites. *Elife* **2021**, *10*, e71636.

(17) Espino-Sanchez, T. J.; Wienkers, H.; Marvin, R. G.; Nalder, S. A.; Garcia-Guerrero, A. E.; VanNatta, P. E.; Jami-Alahmadi, Y.; Mixon Blackwell, A.; Whitby, F. G.; Wohlschlegel, J. A.; Kieber-Emmons, M. T.; Hill, C. P.; Sigala, P. A. Direct tests of cytochrome c and c(1) functions in the electron transport chain of malaria parasites. *Proc. Natl. Acad. Sci. U. S. A.* **2023**, *120*, e2301047120.

(18) Skinner-Adams, T. S.; Fisher, G. M.; Riches, A. G.; Hutt, O. E.; Jarvis, K. E.; Wilson, T.; von Itzstein, M.; Chopra, P.; Antonova-Koch, Y.; Meister, S.; Winzeler, E. A.; Clarke, M.; Fidock, D.

A.; Burrows, J. N.; Ryan, J. H.; Andrews, K. T. Cyclization-blocked proguanil as a strategy to improve the antimalarial activity of atovaquone. *Commun. Biol.* **2019**, *2*, 166.

(19) Babbitt, S. E.; Sutherland, M. C.; San Francisco, B.; Mendez, D. L.; Kranz, R. G. Mitochondrial cytochrome c biogenesis: no longer an enigma. *Trends Biochem. Sci.* **2015**, *40*, 446-455.

(20) Hamel, P.; Corvest, V.; Giege, P.; Bonnard, G. Biochemical requirements for the maturation of mitochondrial c-type cytochromes. *Biochim. Biophys. Acta* **2009**, *1793*, 125-138.

(21) Stevens, J. M.; Daltrop, O.; Allen, J. W.; Ferguson, S. J. C-type cytochrome formation: chemical and biological enigmas. *Acc. Chem. Res.* **2004**, *37*, 999-1007.

(22) Flegontov, P.; Michalek, J.; Janouskovec, J.; Lai, D. H.; Jirku, M.; Hajduskova, E.; Tomcala, A.; Otto, T. D.; Keeling, P. J.; Pain, A.; Obornik, M.; Lukes, J. Divergent mitochondrial respiratory chains in phototrophic relatives of apicomplexan parasites. *Mol. Biol. Evol.* **2015**, *32*, 1115-1131.

(23) Dumont, M. E.; Ernst, J. F.; Hampsey, D. M.; Sherman, F. Identification and sequence of the gene encoding cytochrome c heme lyase in the yeast Saccharomyces cerevisiae. *EMBO J.* **1987**, *6*, 235-241.

(24) San Francisco, B.; Bretsnyder, E. C.; Kranz, R. G. Human mitochondrial holocytochrome c synthase's heme binding, maturation determinants, and complex formation with cytochrome c. *Proc. Natl. Acad. Sci. U. S. A.* **2013**, *110*, E788-797.

(25) Sutherland, M. C.; Mendez, D. L.; Babbitt, S. E.; Tillman, D. E.; Melnikov, O.; Tran, N. L.; Prizant, N. T.; Collier, A. L.; Kranz, R. G. In vitro reconstitution reveals major differences between human and bacterial cytochrome c synthases. *Elife* **2021**, *10*.

(26) Bernard, D. G.; Gabilly, S. T.; Dujardin, G.; Merchant, S.; Hamel, P. P. Overlapping specificities of the mitochondrial cytochrome c and c1 heme lyases. *J. Biol. Chem.* **2003**, *278*, 49732-49742.

(27) Zollner, A.; Rodel, G.; Haid, A. Molecular cloning and characterization of the Saccharomyces cerevisiae CYT2 gene encoding cytochrome-c1-heme lyase. *Eur J Biochem* **1992**, *207*, 1093-1100.

(28) Tjhin, E. T.; Hayward, J. A.; McFadden, G. I.; van Dooren, G. G. Characterization of the apicoplast-localized enzyme TgUroD in Toxoplasma gondii reveals a key role of the apicoplast in heme biosynthesis. *J. Biol. Chem.* **2020**, *295*, 1539-1550.

(29) Bushell, E.; Gomes, A. R.; Sanderson, T.; Anar, B.; Girling, G.; Herd, C.; Metcalf, T.; Modrzynska, K.; Schwach, F.; Martin, R. E.; Mather, M. W.; McFadden, G. I.; Parts, L.; Rutledge, G. G.; Vaidya, A. B.; Wengelnik, K.; Rayner, J. C.; Billker, O. Functional Profiling of a *Plasmodium* Genome Reveals an Abundance of Essential Genes. *Cell* **2017**, *170*, 260-272 e268.

(30) Zhang, M.; Wang, C.; Otto, T. D.; Oberstaller, J.; Liao, X.; Adapa, S. R.; Udenze, K.; Bronner, I. F.; Casandra, D.; Mayho, M.; Brown, J.; Li, S.; Swanson, J.; Rayner, J. C.; Jiang, R. H. Y.;

Adams, J. H. Uncovering the essential genes of the human malaria parasite *Plasmodium falciparum* by saturation mutagenesis. *Science* **2018**, *360*, eaap7847.

(31) Posayapisit, N.; Songsungthong, W.; Koonyosying, P.; Falade, M. O.; Uthaipibull, C.; Yuthavong, Y.; Shaw, P. J.; Kamchonwongpaisan, S. Cytochrome c and c1 heme lyases are essential in *Plasmodium berghei*. *Mol. Biochem. Parasitol.* **2016**, *210*, 32-36.

(32) Babbitt, S. E.; San Francisco, B.; Bretsnyder, E. C.; Kranz, R. G. Conserved residues of the human mitochondrial holocytochrome c synthase mediate interactions with heme. *Biochemistry* **2014**, *53*, 5261-5271.

(33) Mendez, D. L.; Babbitt, S. E.; King, J. D.; D'Alessandro, J.; Watson, M. B.; Blankenship, R. E.; Mirica, L. M.; Kranz, R. G. Engineered holocytochrome c synthases that biosynthesize new cytochromes c. *Proc. Natl. Acad. Sci. U. S. A.* **2017**, *114*, 2235-2240.

(34) Abramson, J.; Adler, J.; Dunger, J.; Evans, R.; Green, T.; Pritzel, A.; Ronneberger, O.; Willmore, L.; Ballard, A. J.; Bambrick, J.; Bodenstein, S. W.; Evans, D. A.; Hung, C. C.; O'Neill, M.; Reiman, D.; Tunyasuvunakool, K.; Wu, Z.; Zemgulyte, A.; Arvaniti, E.; Beattie, C.; Bertolli, O.; Bridgland, A.; Cherepanov, A.; Congreve, M.; Cowen-Rivers, A. I.; Cowie, A.; Figurnov, M.; Fuchs, F. B.; Gladman, H.; Jain, R.; Khan, Y. A.; Low, C. M. R.; Perlin, K.; Potapenko, A.; Savy, P.; Singh, S.; Stecula, A.; Thillaisundaram, A.; Tong, C.; Yakneen, S.; Zhong, E. D.; Zielinski, M.; Zidek, A.; Bapst, V.; Kohli, P.; Jaderberg, M.; Hassabis, D.; Jumper, J. M. Accurate structure prediction of biomolecular interactions with AlphaFold 3. *Nature* **2024**.

(35) Zhang, Y.; Stevens, J. M.; Ferguson, S. J. Substrate recognition of holocytochrome c synthase: N-terminal region and CXXCH motif of mitochondrial cytochrome c. *FEBS Lett.* **2014**, *588*, 3367-3374.

(36) Babbitt, S. E.; San Francisco, B.; Mendez, D. L.; Lukat-Rodgers, G. S.; Rodgers, K. R.; Bretsnyder, E. C.; Kranz, R. G. Mechanisms of mitochondrial holocytochrome c synthase and the key roles played by cysteines and histidine of the heme attachment site, Cys-XX-Cys-His. *J. Biol. Chem.* **2014**, *289*, 28795-28807.

(37) Ganesan, S. M.; Falla, A.; Goldfless, S. J.; Nasamu, A. S.; Niles, J. C. Synthetic RNA-protein modules integrated with native translation mechanisms to control gene expression in malaria parasites. *Nat. Commun.* **2016**, *7*, 10727.

(38) Maruthi, M.; Ling, L.; Zhou, J.; Ke, H. Dispensable Role of Mitochondrial Fission Protein 1 (Fis1) in the Erythrocytic Development of Plasmodium falciparum. *mSphere* **2020**, *5*.

(39) Okada, M.; Rajaram, K.; Swift, R. P.; Mixon, A.; Maschek, J. A.; Prigge, S. T.; Sigala, P. A. Critical role for isoprenoids in apicoplast biogenesis by malaria parasites. *Elife* **2022**, *11*, eLife.73208.

(40) Nicholson, D. W.; Stuart, R. A.; Neupert, W. Biogenesis of cytochrome c1. Role of cytochrome c1 heme lyase and of the two proteolytic processing steps during import into mitochondria. *J. Biol. Chem.* **1989**, *264*, 10156-10168.

(41) Vaca Jacome, A. S.; Rabilloud, T.; Schaeffer-Reiss, C.; Rompais, M.; Ayoub, D.; Lane, L.; Bairoch, A.; Van Dorsselaer, A.; Carapito, C. N-terminome analysis of the human mitochondrial proteome. *Proteomics* **2015**, *15*, 2519-2524.

(42) Young, C. L.; Britton, Z. T.; Robinson, A. S. Recombinant protein expression and purification: a comprehensive review of affinity tags and microbial applications. *Biotechnol J* **2012**, *7*, 620-634.

(43) Rosano, G. L.; Ceccarelli, E. A. Recombinant protein expression in Escherichia coli: advances and challenges. *Front Microbiol* **2014**, *5*, 172.

(44) Evers, F.; Cabrera-Orefice, A.; Elurbe, D. M.; Kea-Te Lindert, M.; Boltryk, S. D.; Voss, T. S.; Huynen, M. A.; Brandt, U.; Kooij, T. W. A. Composition and stage dynamics of mitochondrial complexes in *Plasmodium falciparum*. *Nat. Commun.* **2021**, *12*, 3820.

(45) Maclean, A. E.; Bridges, H. R.; Silva, M. F.; Ding, S.; Ovciarikova, J.; Hirst, J.; Sheiner, L. Complexome profile of *Toxoplasma gondii* mitochondria identifies divergent subunits of respiratory chain complexes including new subunits of cytochrome bc1 complex. *PLoS Pathog.* **2021**, *17*, e1009301.

(46) Hayward, J. A.; Rajendran, E.; Zwahlen, S. M.; Faou, P.; van Dooren, G. G. Divergent features of the coenzyme Q:cytochrome c oxidoreductase complex in *Toxoplasma gondii* parasites. *PLoS Pathog.* **2021**, *17*, e1009211.

(47) Sheokand, P. K.; Pradhan, S.; Maclean, A. E.; Muhleip, A.; Sheiner, L. Plasmodium falciparum Mitochondrial Complex III, the Target of Atovaquone, Is Essential for Progression to the Transmissible Sexual Stages. *Int J Mol Sci* **2024**, *25*.

(48) Balta, V. A.; Stiffler, D.; Sayeed, A.; Tripathi, A. K.; Elahi, R.; Mlambo, G.; Bakshi, R. P.; Dziedzic, A. G.; Jedlicka, A. E.; Nenortas, E.; Romero-Rodriguez, K.; Canonizado, M. A.; Mann, A.; Owen, A.; Sullivan, D. J.; Prigge, S. T.; Sinnis, P.; Shapiro, T. A. Clinically relevant atovaquone-resistant human malaria parasites fail to transmit by mosquito. *Nat. Commun.* **2023**, *14*, 6415.

(49) Goodman, C. D.; Siregar, J. E.; Mollard, V.; Vega-Rodriguez, J.; Syafruddin, D.; Matsuoka, H.; Matsuzaki, M.; Toyama, T.; Sturm, A.; Cozijnsen, A.; Jacobs-Lorena, M.; Kita, K.; Marzuki, S.; McFadden, G. I. Parasites resistant to the antimalarial atovaquone fail to transmit by mosquitoes. *Science* **2016**, *352*, 349-353.

(50) Zhang, Z.; Huang, L.; Shulmeister, V. M.; Chi, Y. I.; Kim, K. K.; Hung, L. W.; Crofts, A. R.; Berry, E. A.; Kim, S. H. Electron transfer by domain movement in cytochrome bc1. *Nature* **1998**, *392*, 677-684.

(51) Crivellone, M. D.; Wu, M. A.; Tzagoloff, A. Assembly of the mitochondrial membrane system. Analysis of structural mutants of the yeast coenzyme QH2-cytochrome c reductase complex. *J. Biol. Chem.* **1988**, *263*, 14323-14333.

(52) Muhleip, A.; Kock Flygaard, R.; Ovciarikova, J.; Lacombe, A.; Fernandes, P.; Sheiner, L.; Amunts, A. ATP synthase hexamer assemblies shape cristae of Toxoplasma mitochondria. *Nat. Commun.* **2021**, *12*, 120.

(53) Hillier, C.; Pardo, M.; Yu, L.; Bushell, E.; Sanderson, T.; Metcalf, T.; Herd, C.; Anar, B.; Rayner, J. C.; Billker, O.; Choudhary, J. S. Landscape of the Plasmodium Interactome Reveals Both Conserved and Species-Specific Functionality. *Cell Rep.* **2019**, *28*, 1635-1647 e1635.

(54) Kranz, R. G.; Richard-Fogal, C.; Taylor, J. S.; Frawley, E. R. Cytochrome c biogenesis: mechanisms for covalent modifications and trafficking of heme and for heme-iron redox control. *Microbiol. Mol. Biol. Rev.* **2009**, *73*, 510-528, Table of Contents.

(55) Allen, J. W.; Jackson, A. P.; Rigden, D. J.; Willis, A. C.; Ferguson, S. J.; Ginger, M. L. Order within a mosaic distribution of mitochondrial c-type cytochrome biogenesis systems? *FEBS J.* **2008**, *275*, 2385-2402.

(56) Holm, L.; Rosenstrom, P. Dali server: conservation mapping in 3D. *Nucleic Acids Res.* **2010**, *38*, W545-549.

(57) Ke, H.; Sigala, P. A.; Miura, K.; Morrisey, J. M.; Mather, M. W.; Crowley, J. R.; Henderson, J. P.; Goldberg, D. E.; Long, C. A.; Vaidya, A. B. The heme biosynthesis pathway is essential for *Plasmodium falciparum* development in mosquito stage but not in blood stages. *J. Biol. Chem.* **2014**, *289*, 34827-34837.

(58) Nagaraj, V. A.; Sundaram, B.; Varadarajan, N. M.; Subramani, P. A.; Kalappa, D. M.; Ghosh, S. K.; Padmanaban, G. Malaria parasite-synthesized heme is essential in the mosquito and liver stages and complements host heme in the blood stages of infection. *PLoS Pathog.* **2013**, *9*, e1003522.

(59) Rizopoulos, Z.; Matuschewski, K.; Haussig, J. M. Distinct Prominent Roles for Enzymes of Plasmodium berghei Heme Biosynthesis in Sporozoite and Liver Stage Maturation. *Infect Immun* **2016**, *84*, 3252-3262.

(60) Goldberg, D. E.; Sigala, P. A. *Plasmodium* heme biosynthesis: To be or not to be essential? *PLoS Pathog.* **2017**, *13*, e1006511.

(61) Rathnapala, U. L.; Goodman, C. D.; McFadden, G. I. A novel genetic technique in Plasmodium berghei allows liver stage analysis of genes required for mosquito stage development and demonstrates that de novo heme synthesis is essential for liver stage development in the malaria parasite. *PLoS Pathog.* **2017**, *13*, e1006396.

(62) Sigala, P. A.; Crowley, J. R.; Henderson, J. P.; Goldberg, D. E. Deconvoluting heme biosynthesis to target blood-stage malaria parasites. *Elife* **2015**, *4*, e09143.

(63) Lill, R.; Stuart, R. A.; Drygas, M. E.; Nargang, F. E.; Neupert, W. Import of cytochrome c heme lyase into mitochondria: a novel pathway into the intermembrane space. *EMBO J.* **1992**, *11*, 449-456.

(64) Medlock, A. E.; Shiferaw, M. T.; Marcero, J. R.; Vashisht, A. A.; Wohlschlegel, J. A.; Phillips, J. D.; Dailey, H. A. Identification of the Mitochondrial Heme Metabolism Complex. *PLoS One* **2015**, *10*, e0135896.

(65) Piel, R. B., 3rd; Dailey, H. A., Jr.; Medlock, A. E. The mitochondrial heme metabolon: Insights into the complex(ity) of heme synthesis and distribution. *Mol Genet Metab* **2019**, *128*, 198-203.

(66) Spillman, N. J.; Beck, J. R.; Ganesan, S. M.; Niles, J. C.; Goldberg, D. E. The chaperonin TRiC forms an oligomeric complex in the malaria parasite cytosol. *Cell Microbiol.* **2017**, *19*, cmi.12719.

(67) Wellems, T. E.; Panton, L. J.; Gluzman, I. Y.; do Rosario, V. E.; Gwadz, R. W.; Walker-Jonah, A.; Krogstad, D. J. Chloroquine resistance not linked to mdr-like genes in a *Plasmodium falciparum* cross. *Nature* **1990**, *345*, 253-255.

(68) Ponnudurai, T.; Leeuwenberg, A. D.; Meuwissen, J. H. Chloroquine sensitivity of isolates of *Plasmodium falciparum* adapted to in vitro culture. *Trop. Geogr. Med.* **1981**, *33*, 50-54.

(69) van den Hoff, M. J.; Moorman, A. F.; Lamers, W. H. Electroporation in 'intracellular' buffer increases cell survival. *Nucleic Acids Res.* **1992**, *20*, 2902.

(70) Lowry, O. H.; Rosebrough, N. J.; Farr, A. L.; Randall, R. J. Protein measurement with the Folin phenol reagent. *J. Biol. Chem.* **1951**, *193*, 265-275.

(71) Altschul, S. F.; Madden, T. L.; Schaffer, A. A.; Zhang, J.; Zhang, Z.; Miller, W.; Lipman, D. J. Gapped BLAST and PSI-BLAST: a new generation of protein database search programs. *Nucleic Acids Res.* **1997**, *25*, 3389-3402.

(72) Sievers, F.; Higgins, D. G. Clustal Omega, accurate alignment of very large numbers of sequences. *Methods Mol. Biol.* **2014**, *1079*, 105-116.

(73) Waterhouse, A. M.; Procter, J. B.; Martin, D. M.; Clamp, M.; Barton, G. J. Jalview Version 2--a multiple sequence alignment editor and analysis workbench. *Bioinformatics* **2009**, *25*, 1189-1191.

(74) Trifinopoulos, J.; Nguyen, L. T.; von Haeseler, A.; Minh, B. Q. W-IQ-TREE: a fast online phylogenetic tool for maximum likelihood analysis. *Nucleic Acids Res.* **2016**, *44*, W232-235.

(75) Jumper, J.; Evans, R.; Pritzel, A.; Green, T.; Figurnov, M.; Ronneberger, O.; Tunyasuvunakool, K.; Bates, R.; Zidek, A.; Potapenko, A.; Bridgland, A.; Meyer, C.; Kohl, S. A. A.; Ballard, A. J.; Cowie, A.; Romera-Paredes, B.; Nikolov, S.; Jain, R.; Adler, J.; Back, T.; Petersen, S.; Reiman, D.; Clancy, E.; Zielinski, M.; Steinegger, M.; Pacholska, M.; Berghammer, T.; Bodenstein, S.; Silver, D.; Vinyals, O.; Senior, A. W.; Kavukcuoglu, K.; Kohli, P.; Hassabis, D. Highly accurate protein structure prediction with AlphaFold. *Nature* **2021**, *596*, 583-589.

(76) *MacPyMOL: A PyMOL-based Molecular Graphics Application for MacOS X*; DeLano Scientific LLC: Palo Alto, CA, 2007. http://www.pymol.org (accessed.

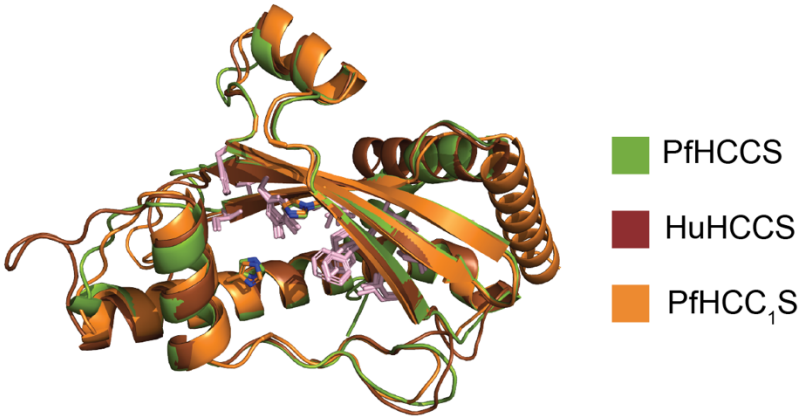

		RMSD Å
PfHCCS ⟷	PfHCC$_1$S	0.812
PfHCCS ⟷	HuHCCS	0.457
PfHCC$_1$S ⟷	HuHCCS	0.885

Figure S1. Structural alignment of the AlphaFold models *P. falciparum* HCCS, *P. falciparum* HCC_1S, and human HCCS.

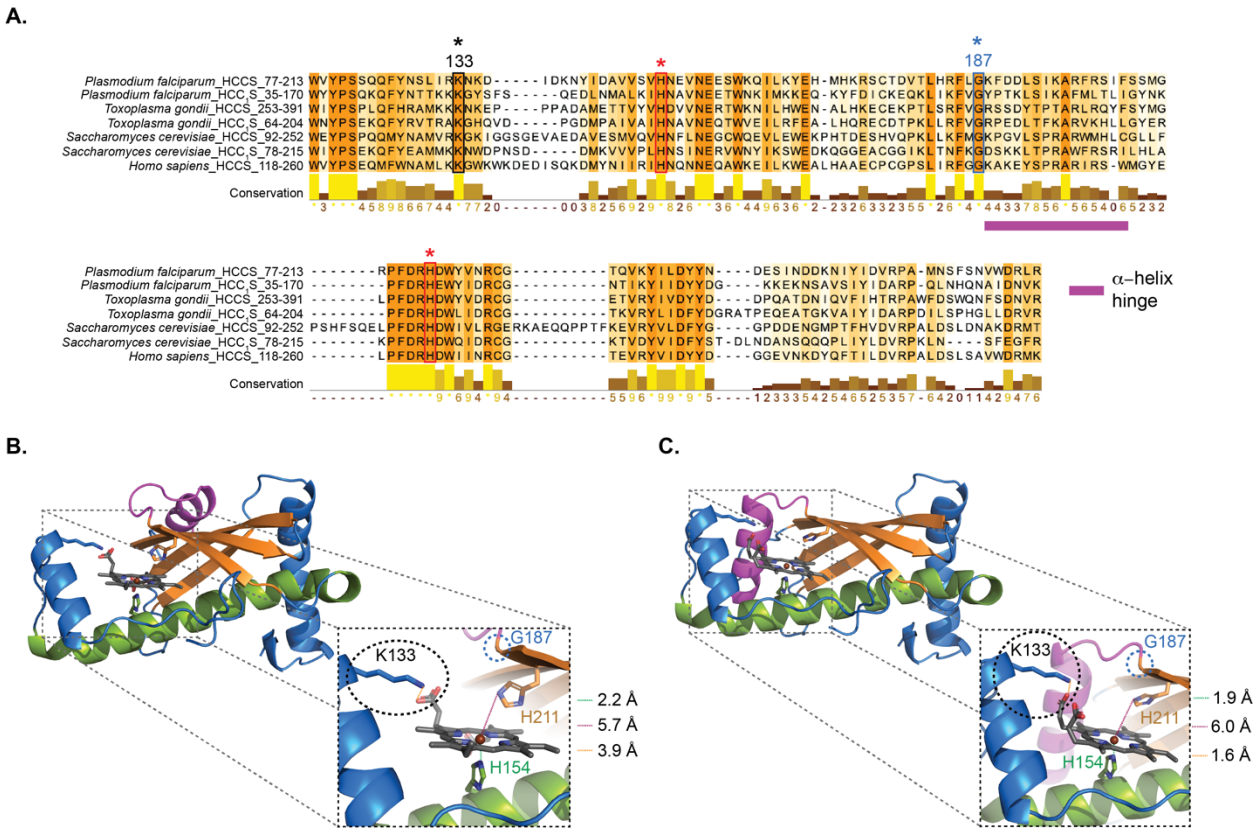

Figure S2. Sequence conservation and conformational variation of HCCS. (A) Sequence alignment of parasite, yeast, and human HCCS homologs highlighting conservation of K92 and G140 (human numbering). (B) and (C) AlphaFold-predicted structural models for *P. falciparum* HCCS with central alpha helix (purple) in two distinct conformations that expose (B) or occlude (C) the heme-binding pocket.

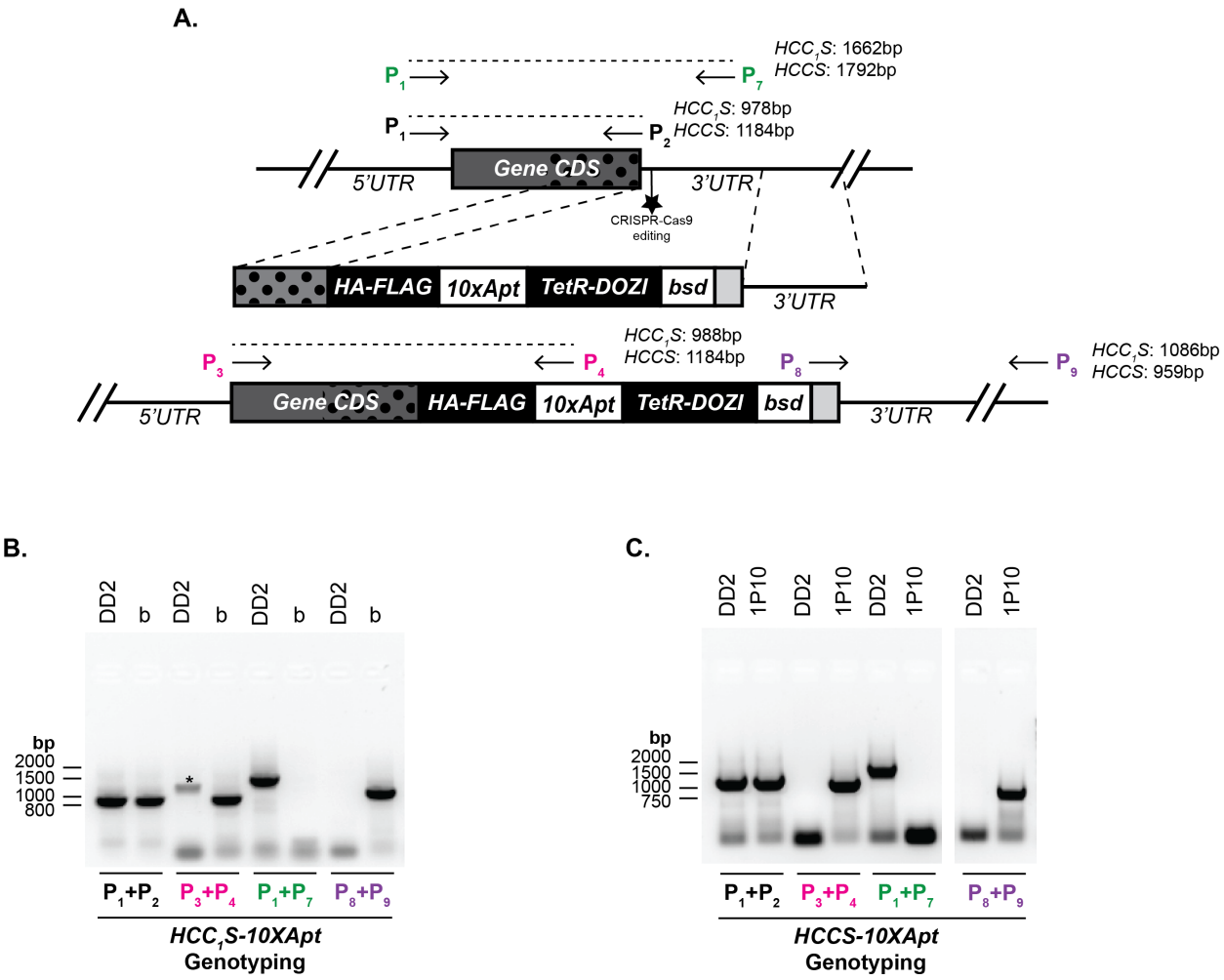

Figure S3. Genotyping HCC_1S and HCCS integrations in Dd2 parasites. (A) Schematic model for editing the chromosomal gene for *P. falciparum* HCCS and HCC_1S to encode a C-terminal HA-FLAG epitope tag fusion and the aptamer/TetR-DOZI system. PCR primer sites are indicated with a "P" along with expected amplicon sizes for primer pairs. (B) Genotype PCR for parental and polyclonal transfectants to edit HCC_1S. Asterisk indicates non-specific amplicon. (C) Genotype PCR for parental and a clonal transfectant to edit HCCS.

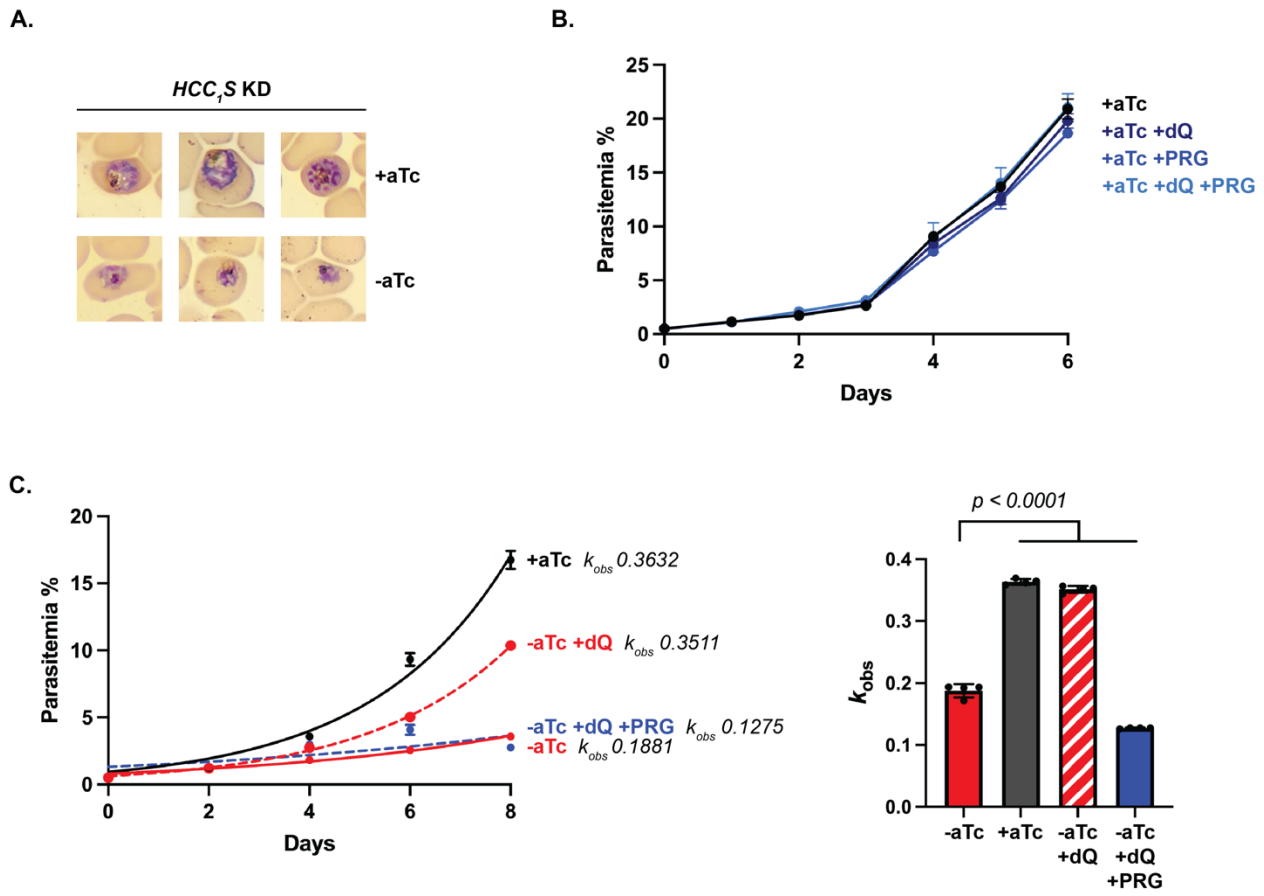

Figure S4. Growth analyses of HCC_1S knockdown parasites. (A) Blood-smear analysis of synchronous HCC_1S knockdown parasites grown 3 days in ±aTc conditions. (B) Synchronous growth analysis of HCC_1S knockdown parasites cultured +aTc, ±15 µM decyl ubiquinone (dQ), and ±1 µM proguanil (PRG). (C) Synchronous growth assay of HCC_1S knockdown parasites cultured ±aTc, ±15 µM dQ, and ±1 µM PRG (data are from Fig. 4B). Parasitemia values from even number days were fit to an exponential growth model in GraphPad Prism to determine the observed rate constant (k_{obs}) for exponential growth. Growth rate constants were determined for each of the four biological replicate samples and used to determine the average ±SD rate constant for each growth condition. Statistical significance (with indicated p values) was determined by two-way ANOVA using GraphPad Prism.

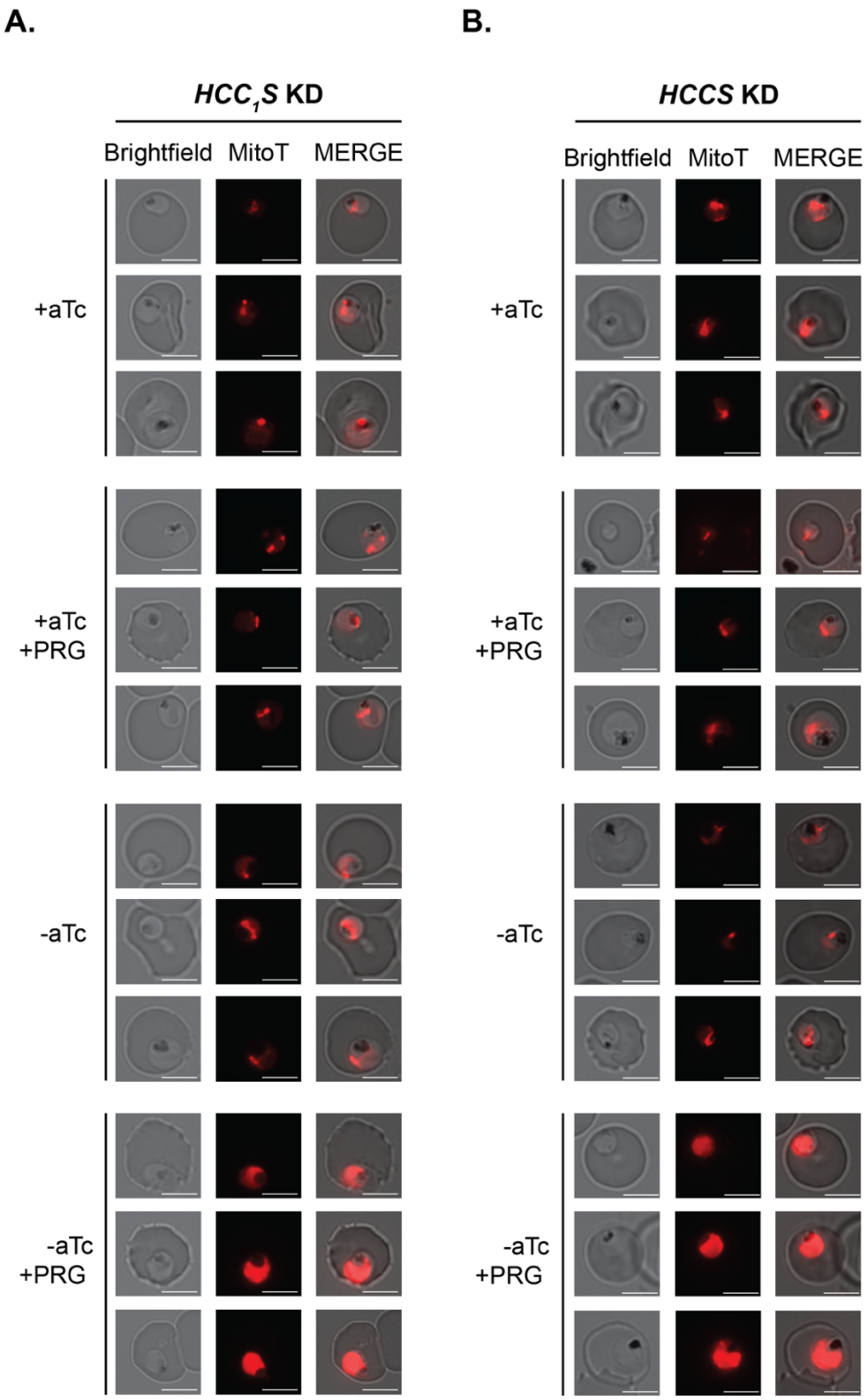

Figure S5. Additional live-parasite microscopy images of HCC_1S (A) and HCCS (B) aptamer/TetR-DOZI Dd2 parasites cultured 5 days ±aTc/+dQ and 1 µM proguanil (PRG) and stained with 1 nM with MitoTracker Red (MitoT). Scale bars represent 5 µm.

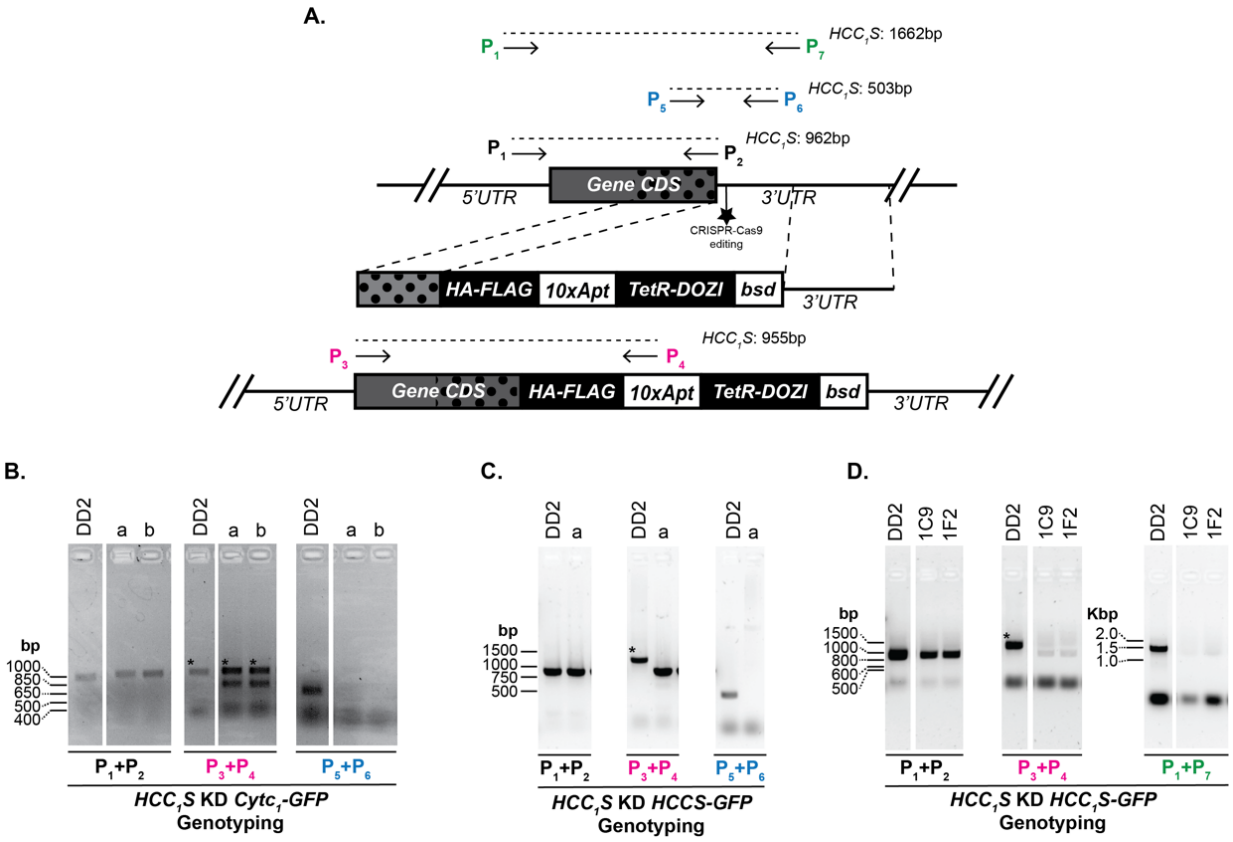

Figure S6. Genotyping HCC_1S integrations in Dd2 parasites transfected with plasmids for episomal expression. (A) Schematic model for editing the chromosomal gene for *P. falciparum* HCC_1S to encode a C-terminal HA-FLAG epitope tag fusion and the 10x aptamer/TetR-DOZI system. PCR primer sites are indicated with a "P" along with expected amplicon sizes for primer pairs. (B) Genotype PCR for parental and polyclonal transfectants (a and b) to edit HCC_1S in parasites transfected with a plasmid for episomal expression of cyt c_1-GFP. (C) Genotype PCR for parental and polyclonal transfectant a to edit HCC_1S in parasites transfected with a plasmid for episomal expression of HCCS-GFP. (D) Genotype PCR for parental and clonal transfectants 1C9 and 1F2 to edit HCC_1S in parasites transfected with a plasmid for episomal expression of HCC_1S-GFP. Non-specific amplicons are indicated with asterisks.

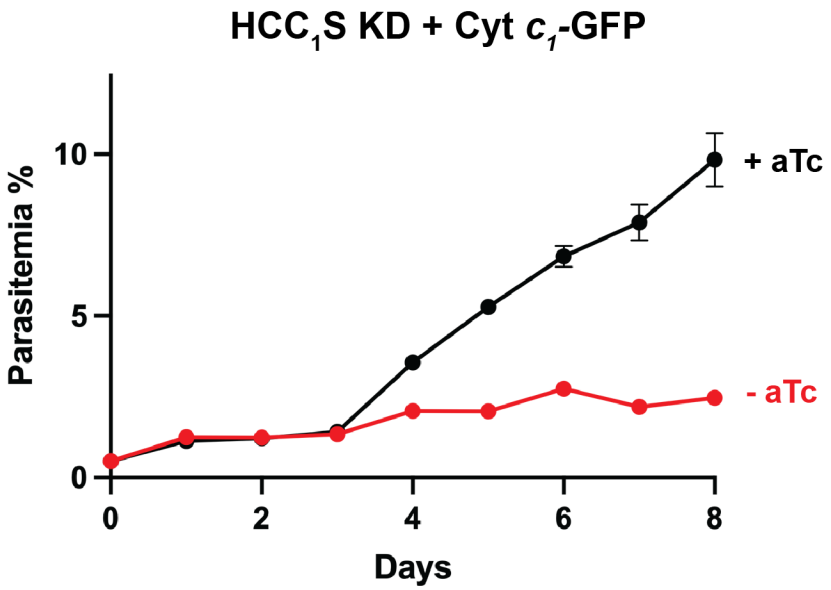

Figure S7. Synchronous growth assay of Dd2 parasites tagged for conditional knockdown (KD) of HCC_1S expression in ±anhydrotetracycline (aTc) conditions and transfected with a plasmid for episomal expression of cyt c_1-GFP. Data points and error bars represent the average ± SD of biological triplicates.

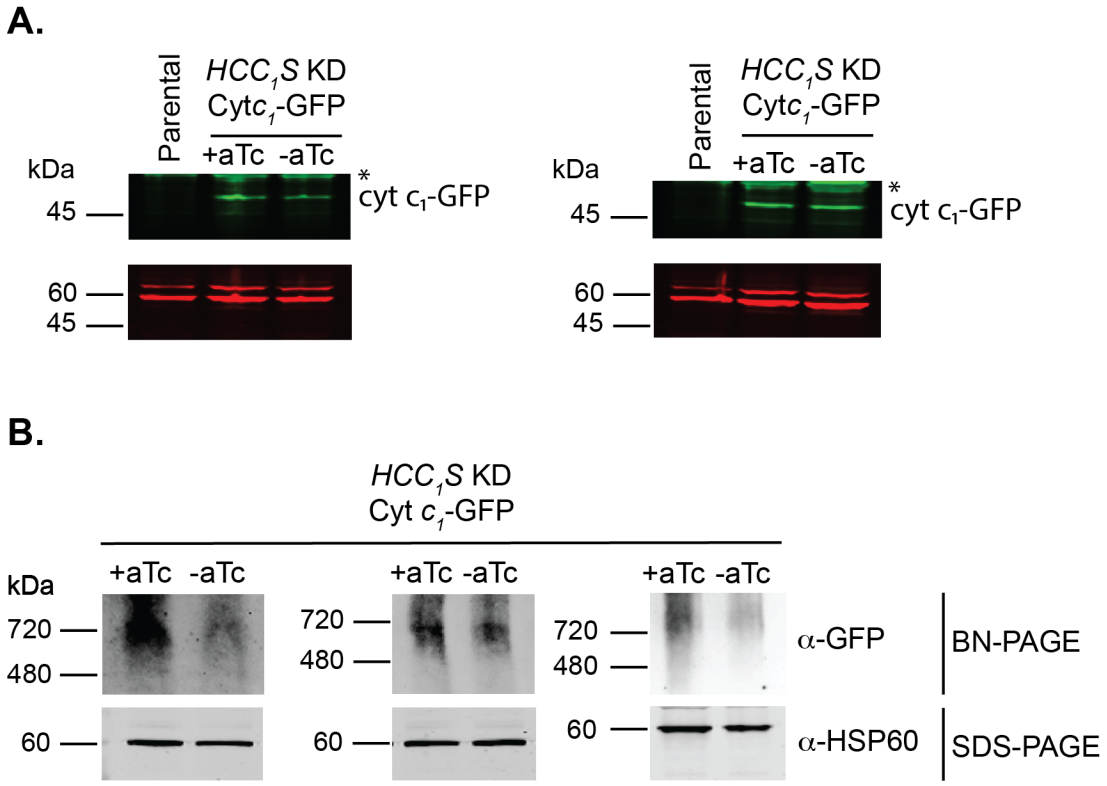

Figure S8. Additional western blot (WB) images from biological replicate growth assays of HCC_1S knockdown Dd2 parasites episomally expressing cyt c_1-GFP and grown 3 days ±aTc . (A) SDS-PAGE/WB images from independent growth assays (left and right) probed with α-GFP (green) and α-Hsp60 (red) antibodies. The asterisk indicates non-specific background bands visible in parental parasites (see Fig. S9 for uncropped images). (B) Blue native-PAGE/WB analysis of cyt c_1-GFP and SDS-PAGE/WB analysis of HSP60 expression levels in HCC_1S knockdown parasites cultured 5 days ±aTc/+dQ. 20 µg of total protein from mitochondrial lysates were loaded for each lane. Blots were probed with α-GFP or α-HSP60 antibodies.

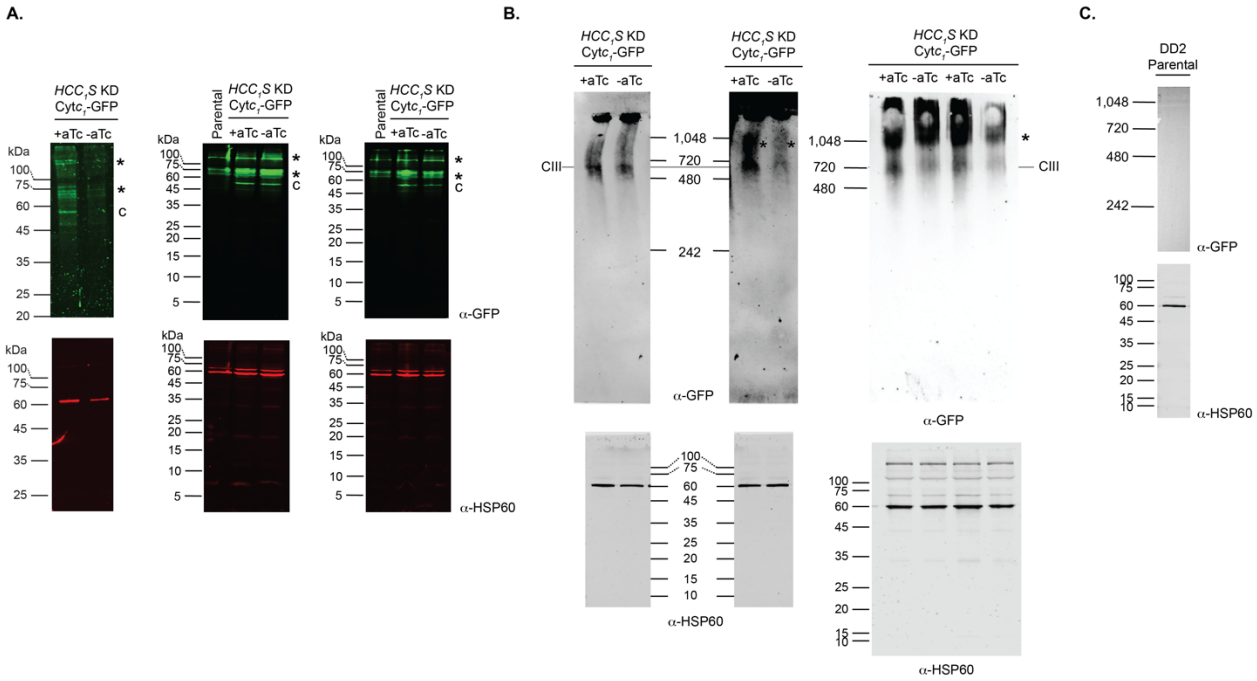

Figure S9. Uncropped western blot images. (A) SDS-PAGE/WB analysis of cyt c_1-GFP levels in HCC_1S knockdown (KD) Dd2 parasites cultured in ±aTc/+dQ conditions and probed with anti-GFP or anti-HSP60 antibodies. Asterisks label non-specific anti-GFP signal detected in parental parasites. The letter "c" indicates the specific band for cyt c_1-GFP. (B) BN-PAGE/WB analyses of cyt c_1-GFP levels in HCC_1S knockdown (KD) Dd2 parasites cultured in ±aTc/+dQ conditions and probed with anti-GFP or anti-HSP60 antibodies. The lower panels are SDS-PAGE/WB analyses for HSP60 of identical samples as loaded in equivalent lanes in the upper panel images. Asterisks in reflect anti-GFP signal that does not correspond to the known size for Complex III ~700 kDa. (C) The upper panel is a BN-PAGE/WB analysis of parental Dd2 parasites probed with an anti-GFP antibody. The lower panel is an SDS-PAGE/WB of an identical sample from parental Dd2 parasites probed with anti-HSP60 antibody.

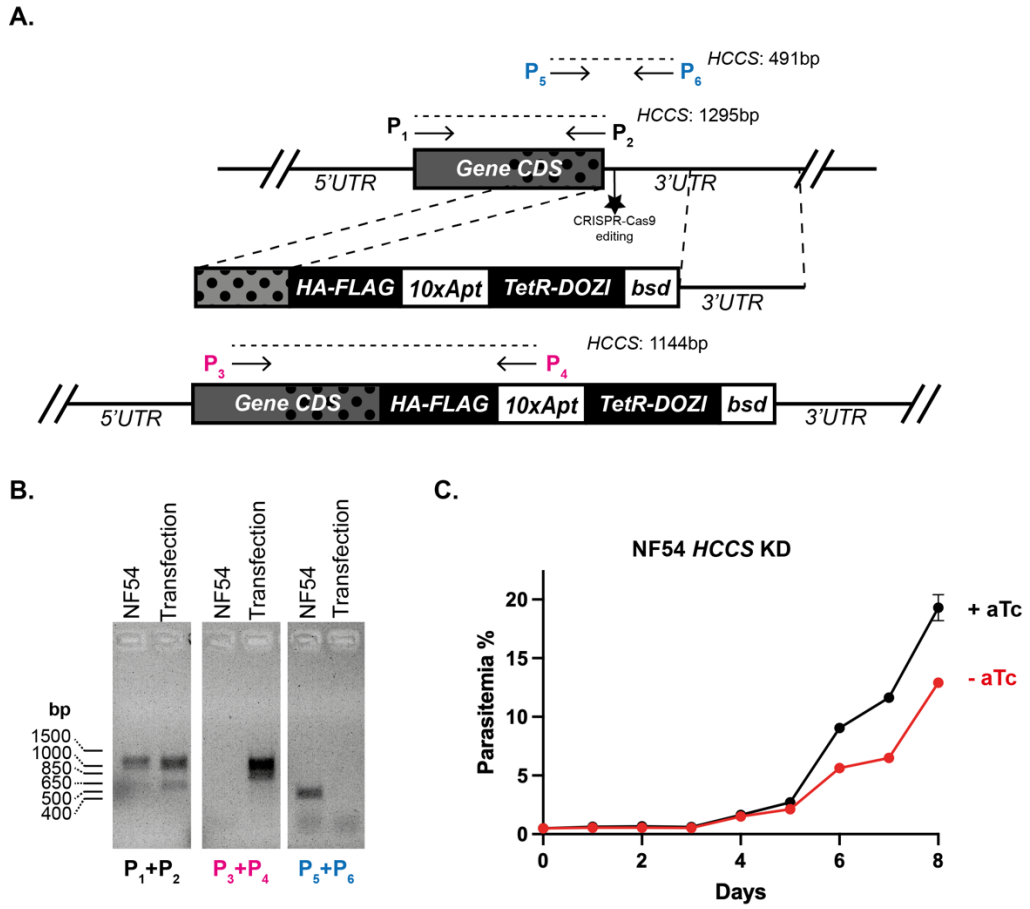

Figure S10. Genotyping HCCS integration in NF54 parasites. (A) Schematic model for editing the chromosomal gene for *P. falciparum* HCCS to encode a C-terminal HA-FLAG epitope tag fusion and the aptamer/TetR-DOZI system. PCR primer sites are indicated with a "P" along with expected amplicon sizes for primer pairs. (B) Genotype PCR for parental and polyclonal transfectants to edit HCC_1S. (C) Synchronous growth assay of NF54 parasites tagged for conditional knockdown (KD) of HCCS expression in ±anhydrotetracycline (aTc) conditions. Data points and error bars represent the average ± SD of biological triplicates.

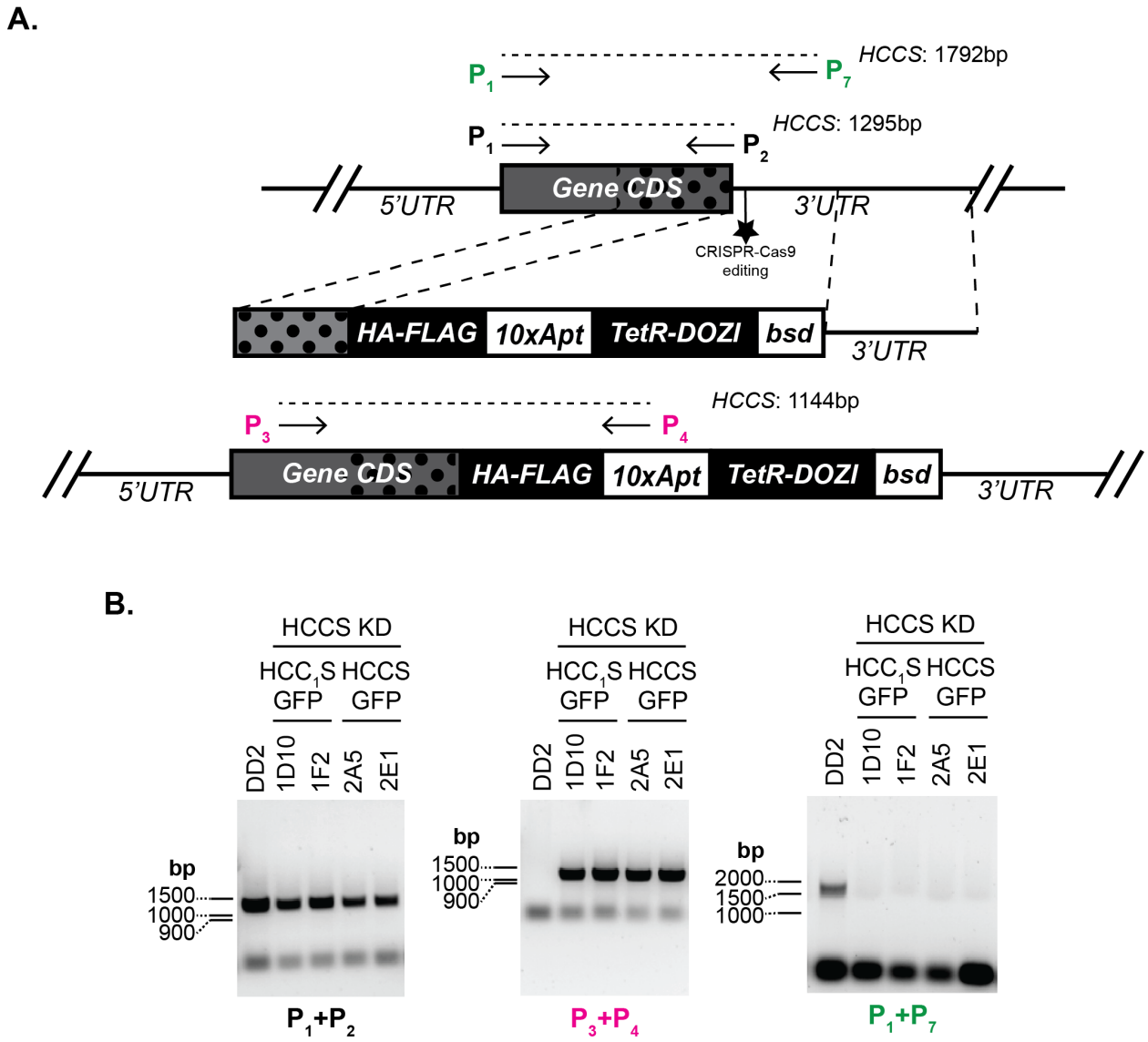

Figure S11. Genotyping HCCS integrations in Dd2 parasites transfected with plasmids for episomal expression. (A) Schematic model for editing the chromosomal gene for *P. falciparum* HCCS to encode a C-terminal HA-FLAG epitope tag fusion and the 10x aptamer/TetR-DOZI system. PCR primer sites are indicated with a "P" along with expected amplicon sizes for primer pairs. (B) Genotype PCR for parental and clonal transfectants to edit HCCS in parasites episomal expressing HCC_1S-GFP or HCCS-GFP.

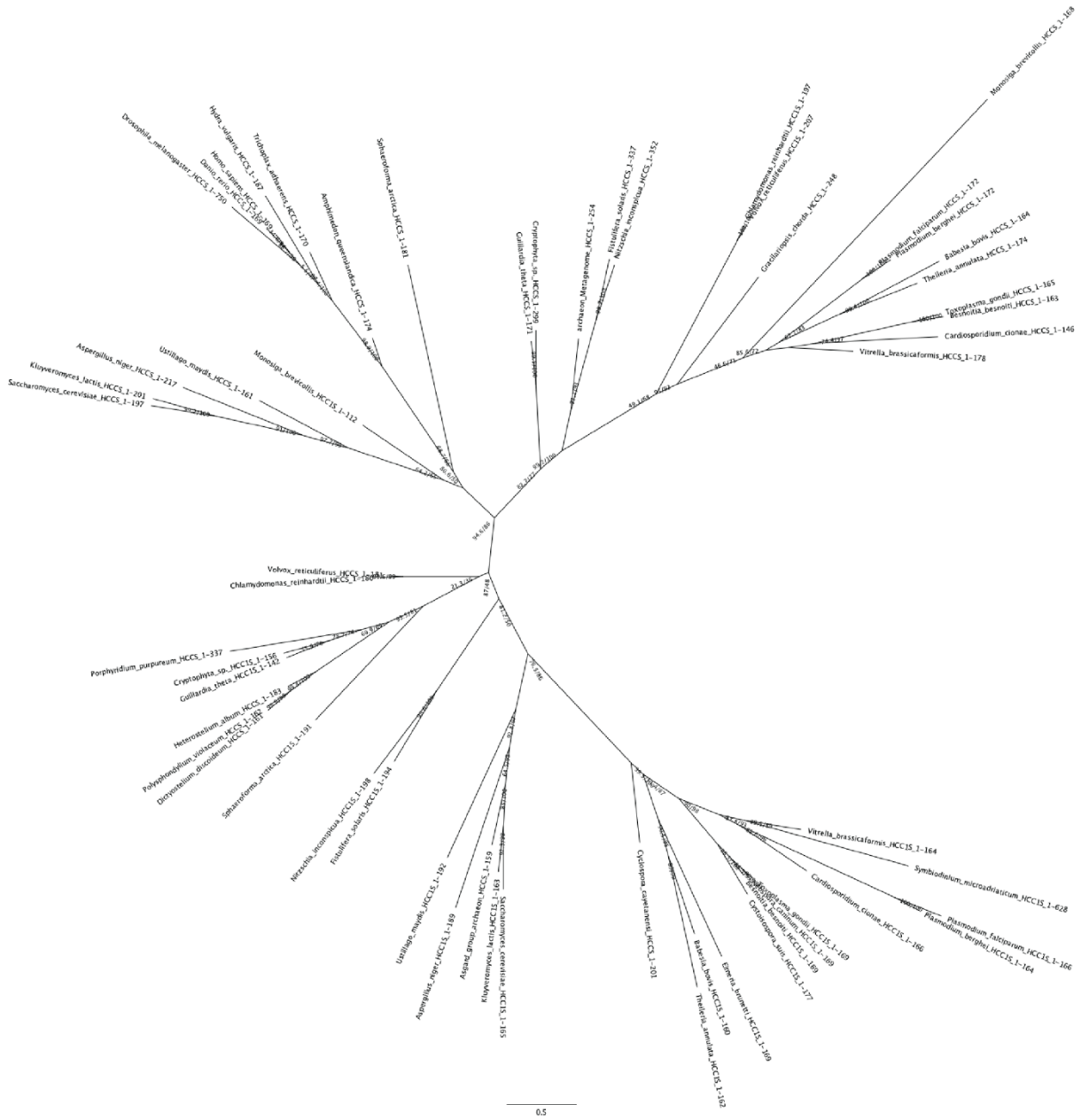

Figure S12. Raw phylogenetic tree based on sequence comparison of *P. falciparum* HCCS and HCC_1S relative to diverse eukaryotes. This raw tree was used to create Figure 2B.

Table S1. List of organisms and HCCS/HCC_1S protein sequences aligned in Fig. S12.

Organism	GenBank
Plasmodium falciparum	KAF4327347.1
Plasmodium falciparum	KAF4327070.1
Plasmodium berghei	XP_034424219.1
Plasmodium berghei	XP_034420526.1
Toxoplasma gondii	KAF4646083.1
Toxoplasma gondii	XP_002364614.2
Eimeria brunetti	CDJ51885.1
Neospora caninum	XP_003885328.1
Cystoisospora suis	PHJ20471.1
Symbiodinium microadriaticum	OLQ04208.1
Cyclospora cayetanensis	XP_022588510.2
Babesia bovis	XP_001612270.1
Babesia bovis	EDO07243.2
Theileria annulata	XP_951931.1
Theileria annulata	XP_953889.1
Cardiosporidium cionae	KAF8819734.1
Cardiosporidium cionae	KAF8822908.1
Besnoitia besnoiti	XP_029222774.1
Besnoitia besnoiti	XP_029218356
Vitrella brassicaformis	CEM02166.1
Vitrella brassicaformis	CEL92815.1
Chlamydomonas reinhardtii	XP_042915786.1
Chlamydomonas reinhardtii	XP_042918551.1
Volvox reticuliferus	GIL82651.1
Volvox reticuliferus	GIL70918.1
Porphyridium purpureum	KAA8493688.1
Gracilariopsis chorda	PXF40648.1
Asgard group archaeon	MCP8720244.1
archaeon (Metagenome)	RYH06097.1
Dictyostelium discoideum	XP_643563.1
Polysphondylium violaceum	KAF2072366.1
Heterostelium album	XP_020432267.1
Heterostelium album	XP_020427510.1
Fistulifera solaris	GAX15878.1
Fistulifera solaris	GAX20154.1
Nitzschia inconspicua	KAG7370135.1
Nitzschia inconspicua	KAG7361072.1
Guillardia theta	XP_005830278.1
Guillardia theta	XP_005839063.1
Cryptophyta sp.	KAJ1487503.1
Cryptophyta sp.	KAJ1494728.1
Kluyveromyces lactis	CAH01636.1
Kluyveromyces lactis	CAG98941.1
Ustillago maydis	XP_757596.1
Ustillago maydis	XP_760849.1
Aspergillus niger	XP_001400653.1
Aspergillus niger	XP_001401520.1
Saccharomyces cerevisiae	NP_009361.1
Saccharomyces cerevisiae	NP_012836.1
Drosophila melanogaster	AAF55946.1
Danio rerio	NP_958859.1
Homo sapiens	NP_001116080.1
Monosiga brevicollis	XP_001749606.1
Monosiga brevicollis	XP_001748514.1
Sphaeroforma arctica	XP_014157735.1
Amphimedon queenslandica	XP_003385371.1
Trichoplax adhaerens	XP_002114862.1
Hydra vulgaris	XP_047122850.1

Table S2. List of primers.

Primer	Sequence	
#51	CCCCTTTCCGGGCGCGCCGTATGTATTGAATACATTTGTTTCG	AscI restriction site
#52	CGGGCATCATATTTCTTTCGCTTAAGCCTTTATTTATTTGTATATGTGCATAAAT AAATG	AflII restriction site
#53	CATTTATTTATGCACATATACAAATAAATAAAGGCTTAAGCGAAAGAAATATGA TGCCCG	AflII restriction site
#54	CATAAGGATAGACGTCTTTAAATAATTCATCTTTTTTTACATACTTAAAG	AatII restriction site
#55	CCCCTTTCCGGGCGCGCCCTTTCTTTTTGTGCATCATAAATG	AscI restriction site
#56	TATATTTTCTTTTTTTTGTTCATTCATCTTAAGGTAATTCTGTATTAACAAAAACA TATC	AflII restriction site
#57	GATATGTTTTTGTTAATACAGAATTACCTTAAGATGAATGAACAAAAAAAAGA AAATATA	AflII restriction site
#58	CATAAGGATAGACGTCAAAAAGGTTATTTAAAAATCTACAAATCTTTATATAAA TAATTTTAAC	AatII restriction site
Primers for gRNAs		
HCCS_gRNA1_F	TAAGTATATAATATTTAACAAAAATTGTGAAAAATGTTTTAGAGCTAGAA	gRNA sequence in red
HCCS_gRNA1_R	TTCTAGCTCTAAAACATTTTTCACAATTTTTGTTAGCAATATTATATACTTA	
HCCS_gRNA2_F	TAAGTATATAATATTGCAAATGTGCAACAAACAATGTTTTAGAGCTAGAA	gRNA sequence in red
HCCS_gRNA2_R	TTCTAGCTCTAAAACATTGTTTGTTGCACATTTGCGCAATATTATATACTTA	
HCC1S_gRNA_F	TAAGTATATAATATTTTATTTATATAAAGATTTGTGTTTTAGAGCTAGAA	gRNA sequence in red
HCC1S_gRNA_R	TTCTAGCTCTAAAACACAAATCTTTATATAAATAAGCAATATTATATACTTA	
Primers for genotyping		
#83_P4	CCCAGGCCTCTAGTTTAC	To genotype pMG74 integration
5'PfHsp60 Rv1_P8	ACTATGGAATACTAAATATATATCCAATGGCCCCTTTCCG	To genotype pMG74 integration
#77_P1	CTTATAAGGAACAAAAGCGAAATAAATAAATATGCAGAATTTAAGTCCAGC	To genotype *HCCS* KD
#54_P2	CATAAGGATAGACGTCTTTAAATAATTCATCTTTTTTTACATACTTAAAG	To genotype *HCCS* KD
#53_P3	CATTTATTTATGCACATATACAAATAAATAAAGGCTTAAGCGAAAGAAATATGA TGCCCG	To genotype *HCCS* KD
PfHCCS Fw2_P5	TCAAATGTCTGGGACAGATTGCGTTACCCCTTTTATGA	To genotype *HCCS* KD
PfHCCS Rv2_P6	ATGAACAACCCAATTGTTTGTTGCACATTTGCAACCA	To genotype *HCCS* KD
PfHCCS Rv7_P7	CCACGTTCTTATATTTAAATGTATTCCTAAAAATAAGCGTG	To genotype *HCCS* KD
PfHCCS Rv9_P9	TTAAAAAATAATGAATTGTCATCTGATTTAGACAAATGTG	To genotype *HCCS* KD
#86_P1	CAACTTAAAAGAAAAAAAATTAAATCATATAAAGAAAAAATATAC	To genotype *HCC_1S* KD
#58_P2	CATAAGGATAGACGTCAAAAAGGTTATTTAAAAATCTACAAATCTTTATATAAA TAATTTTAAC	To genotype *HCC_1S* KD
#57_P3	GATATGTTTTTGTTAATACAGAATTACCTTAAGATGAATGAACAAAAAAAAGA AAATATA	To genotype *HCC_1S* KD
PfHCC$_1$S Fw1_P5	TTCTGCAGTCTCAATTTATATTGATGCCAGACCA	To genotype *HCC_1S* KD
PfHCC$_1$S Rv1_P6	ATGTAAATTTAACAAATCTGTTAAAAATATATGAACGAAATAA	To genotype *HCC_1S* KD
PfHCC$_1$S Rv4_P7	GACAAGAATATACTTGGCGCAAATTAATTATATATACATACC	To genotype *HCC_1S* KD
PfHCC$_1$S Rv4_P9	AGGAAGGTTTTATTTTATCATTTTATTTTGCAACAAATCC	To genotype *HCC_1S* KD
Primers for RT-qPCR		
HCCS_qF1	TGGGATGTTCAGATGGAACGAA	
HCCS_qR1	AGACATTGGGAATCTCGGGC	
HCC$_1$S_qF1	AGTTGGTACTATCCATCCCAGA	
HCC$_1$S_qR1	AATCTTCTTGAGAGAAGGAGTAACC	
I5P_qF1	GACATAAGTTTAGTAGGTCG	
I5P_qR1	TTCTGACTCCACATCATTTG	
ADSL_qF1	GGAAATCCATAGACAAACAATG	
ADSL_qR1	TCCTGTGAGAAGTGCTCCAC	